Application of Differential Geometry in Spherical Harmonics Domain

Saurabh Kataria and Arun Parthasarathy with Lalan Kumar and Prof. Rajesh M. Hegde

CONTENTS

Saurabh Kataria and Arun Parthasarathy are currently junior undergraduate students of Department of Electrical Engineering, Indian Institute of Technology, Kanpur. Lalan Kumar, who is the project guide, is currently a Ph.D. scholar under Prof. Rajesh M. Hegde, who is the project supervisor.

NOTATIONS

A, a	Scalar
$\underline{A}, \underline{a}$	Column vector
$\mathbb{A}$	Matrix
$\mathbb{A}^T$	Transpose
$\mathbb{A}^H$	Hermitian transpose
$\|\mathbb{A}\|$	Norm of a matrix
$|a|, |A|$	Magnitude of a number
$\odot$	Hadamard product
$\exp(\mathbb{A})$	Element wise exponential of a matrix
$\text{expm}(\mathbb{A})$	Matrix exponential
$\text{Tr}(\mathbb{A})$	Trace of a matrix
$\det(\mathbb{A})$	Determinant of a matrix
$\mathbb{I}_N$	Identity matrix of dimension $N \times N$
$\mathbb{R}$	Set of real numbers
$\mathfrak{C}$	Set of complex numbers
$\mathcal{L}[\mathbb{A}]$	Subspace spanned by columns of $\mathbb{A}$

ABBREVIATIONS

CRB	Cramer Rao Bound
DF	Direction Finding
DOA	Direction Of Arrival
DSHD	Differential Spherical Harmonics Domain
DSH-MUSIC	Differential Spherical Harmonics-MUSIC
FOV	Field Of View
MVDR	Minimum Variance Distortion-less Response
NLDR	Non-Linear Dimensionality Reduction
SHD	Spherical Harmonics Domain
SNR	Signal-to-Noise Ratio
ULA	Uniform Linear Array
UCA	Uniform Circular Array

I. INTRODUCTION

DIFFERENTIAL geometry is a well-known branch of mathematics that uses the techniques of differential calculus, integral calculus and linear algebra in geometry problems. The use of differential geometry in *array signal processing* gives us tools to investigate manifold in terms of parameters like curvature and rate of change of arc-length (in case of manifold curve) to calculate detection and resolution thresholds and even implement DF algorithms like MUSIC for a given sensor geometry. Array of various geometries are available now-a-days of which *spherical array* enjoys a full 3D FOV and symmetry, due to which it is one of the most widely used array. In this report, tools of differential geometry are employed to investigate spherical array which are conventionally studied in spherical harmonics domain. Some useful insights have been formed by performing CRB-analysis and MUSIC on a 32-sensor spherical array.

II. DIFFERENTIAL GEOMETRY OF MANIFOLD CURVES

A. Data Model

Consider the following data model with N omnidirectional sensors and M sources:

$$\underline{x}(t) = \mathbb{A}\underline{m}(t) + \underline{n}(t) \tag{1}$$

where $\underline{x}(t)$ is the $(N \times 1)$ vector containing output from all sensors, $\underline{m}(t)$ is the $(M \times 1)$ vector containing amplitude of signals, $\underline{n}(t)$ is the $(N \times 1)$ vector consisting of additive baseband white noise from each sensor and $\mathbb{A}$ $(N \times M)$

is called the *steering matrix*.

$$\mathbb{A} = \exp(-j\mathbf{r}^T\mathbf{k}) \tag{2}$$

Position vector matrix $(3 \times N)$, as the name suggests, comprises position vectors of each sensor while assuming the origin of the coordinate system to be at the centroid of the array. Throughout the report, this assumption is strictly followed.

$$\mathbf{r}^T = [\underline{r}_x, \underline{r}_y, \underline{r}_z] \tag{3}$$

Wavenumber matrix is represented by the following expression:

$$\mathbf{k} = [\underline{k}_1, \underline{k}_2, ..., \underline{k}_M] \tag{4}$$

Each column $\underline{k}_m$ of the above matrix is a *wavenumber vector* pointing towards the DOA of the mth signal. Wavenumber vector is formally defined as:

$$\underline{k}_m = \frac{2\pi}{\lambda}[\sin(\theta_m)\cos(\phi_m), \sin(\theta_m)\sin(\phi_m), \cos(\theta_m)]^T \text{ m}^{-1} \tag{5}$$

where λ is the wavelength of the carrier wave of mth signal. However, we can get the following expression by changing its unit:

$$\underline{k}_m = \pi[\sin(\theta_m)\cos(\phi_m), \sin(\theta_m)\sin(\phi_m), \cos(\theta_m)]^T \quad (\lambda/2 \text{ m})^{-1} \tag{6}$$

To maintain dimensional consistency in equation (2), position vector of the sensors must be taken in a different unit which is $(\lambda/2)$ m.

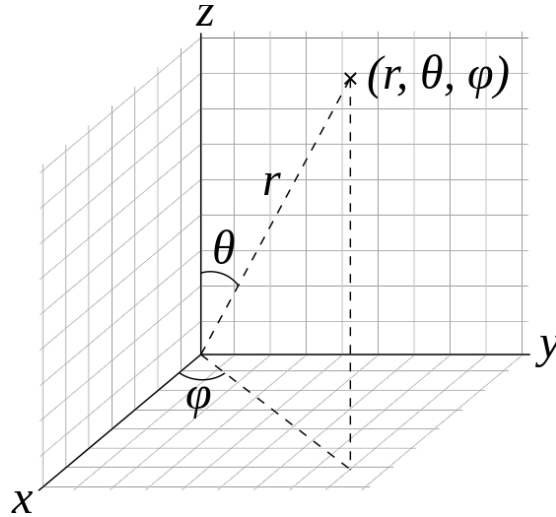Coordinate system used throughout the report is shown here in Fig. 1.

Fig. 1. Elevation: $\theta \in [0, \pi]$ and azimuth: $\phi \in [0, 2\pi]$

B. Array Manifold

Steering matrix defined in previous section has M columns. Each column $\underline{\mathbf{a}}_m$ of that matrix is called *steering vector* corresponding to the mth DOA. Since the number of DOAs are generally finite, there will be finitely many columns in the steering matrix. In general, steering vector can be found out for any direction (θ, ϕ). The locus of steering vector while varying (θ, ϕ) across every point in the FOV is a geometrical object called *array manifold*. Since the dimension of steering vector is $N \times 1$, the manifold will be embedded in an N-dimensional complex space. In other words, manifold consists of steering vectors corresponding to every possible DOA and therefore, every time some points (vectors) in the manifold will always correspond to the actual DOA. In DF algorithms, the main aim is to identify those vectors. The shape of the manifold, whether it is a curve or a surface, depends on the number of directional parameters involved in the expression for steering vector.

Steering vector $(N \times 1)$ can be mathematically expressed as:

$$\underline{\mathbf{a}}_m(\theta_m, \phi_m) = \exp\{-j(\underline{r}_x \sin(\theta_m)\cos(\phi_m) + \underline{r}_y \sin(\theta_m)\sin(\phi_m) + \underline{r}_z \cos(\theta_m))\} \tag{7}$$

For any linear array placed on x-axis, FOV is $\phi \in [0, \pi]$ which is independent of θ because of front-back ambiguity (a drawback of linear arrays). For a planar array placed on x-y plane, FOV is $\phi \in [0, 2\pi], \theta \in [0, \pi/2]$ (again there is a limitation in FOV due to its planar structure). And for a three-dimensional array, FOV is $\phi \in [0, 2\pi], \theta \in [0, \pi]$. (That is, any value of (θ, ϕ)) is allowed as a DOA.)

From the above it is clear that in the case of linear array, there is only one parameter involved i.e. ϕ whereas in the case of planar or three-dimensional array, there are two parameters involved, ϕ and θ. This means that for a linear array, there will be only one parameter in the steering vector and its locus will generate a curve which is called the *manifold curve*. Similar arguments can be made to conclude that for a two- or three-dimensional array, manifold will be a surface (known as *manifold surface*).

Manifold curve is formally defined as:

$$\mathcal{A} \triangleq \{\underline{\mathbf{a}}(\phi) \in \mathfrak{C}^N, \forall \phi : \phi \in \Omega_\phi\} \tag{8}$$

where Ω_ϕ is the parameter space or the FOV. There is a need for re-parametrisation of the manifold curve in terms of a new parameter s, which denotes the *arc-length* of the curve (see Fig. 2) An appropriate reference point is chosen which is $s = 0, \phi = 0$.

The expression for arc-length is as follows:

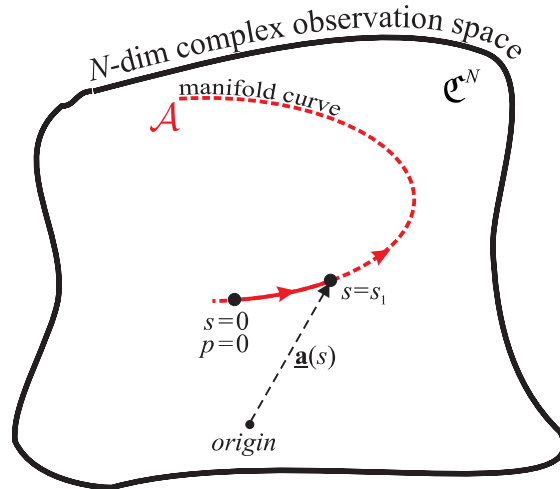$$s(\phi) \triangleq \int_0^s \|\underline{\dot{\mathbf{a}}}(\phi)\| d\phi \tag{9}$$

Fig. 2. Manifold parameterization in terms of arc length s

The benefit of re-parametrisation of $\underline{\mathbf{a}}(\phi)$ in terms of s is that s is an invariant parameter and the norm of the first derivative of $\underline{\mathbf{a}}$ w.r.t. to s is a constant $\forall s$ as shown below:

$$\|\underline{\mathbf{a}}'(s)\| = \left\|\frac{d\underline{\mathbf{a}}(s)}{ds}\right\| = \left\|\frac{d\underline{\mathbf{a}}(\phi)/dp}{ds/dp}\right\| = \frac{\|\underline{\dot{\mathbf{a}}}(\phi)\|}{\dot{s}(\phi)} = \frac{\dot{s}(\phi)}{\dot{s}(\phi)} = 1 \tag{10}$$

Parametrisation can be physically understood through following statements. The first derivative of $\underline{\mathbf{a}}(\phi)$ can be thought of as velocity. Then, its norm should signify speed. Also, if ϕ is considered to be analogous with time, it can be said that speed is being integrated w.r.t to time to give distance covered, which is nothing here but the arc-length.

C. Dimensionality Reduction

Consider the one-dimensional complex plane or the *Argand Plane* where two complex vectors are required to span the whole plane or in other words, to represent any complex vector in that space. This statement can be generalised to an N-dimensional complex space (in case of manifolds) where at most $2N$ vectors should be required to represent any vector. The number $2N$ is called *dimensionality*. Symmetry is something which can be exploited to reduce the *dimensionality* which, in turn, reduces complexity of the analysis. For the case of linear arrays, reduced dimension d is expressed as follows:

$$d = \begin{cases} 2N - m & \text{if } \nexists \text{ sensor at the array centroid} \\ 2N - m - 1 & \text{otherwise} \end{cases} \quad (11)$$

where m is the number of symmetrical pair of sensors plus the one at the centroid (if it exists). Alternatively, it can be said that *dimensionality* is the least number of vectors required to represent manifold. Note that the number of components in steering vector, which is N, cannot be changed. Therefore, the manifold which previously required $2N(N \times 1)$ vectors for its representation now only requires d such vectors.

D. Orthonormal Coordinate System

In $\mathcal{R}^3$ a *fixed* orthonormal coordinate system or a *fixed* frame is used viz. $(\hat{i}, \hat{j}, \hat{k})$. In $\mathfrak{C}^N$ also, a system is required. The fundamental difference would be that in $\mathfrak{C}^N$, the frame or the coordinate vector system will not be fixed, it will change at every point on the manifold curve and hence will be called *moving frame*. (see Fig. 3) At $s = 0$, the matrix containing the coordinate vectors will be denoted by $\mathbb{U}(0)$, and at any general point s, it will be $\mathbb{U}(s)$. Following relation can be used to determine coordinate system at any point:

$$\mathbb{U}(s) = \mathbb{U}(0)\mathbb{F}(s) = [\underline{u}_1(s), \underline{u}_2(s), .., \underline{u}_d(s)] \quad (12)$$

where $\mathbb{F}(s)$ is called *Frame Matrix*. It is a real orthogonal transformation matrix that involve rotation of $\mathbb{U}(0)$ to produce $\mathbb{U}(s)$ at any point s. Clearly $\mathbb{F}(0) = \mathbb{I}_d$.
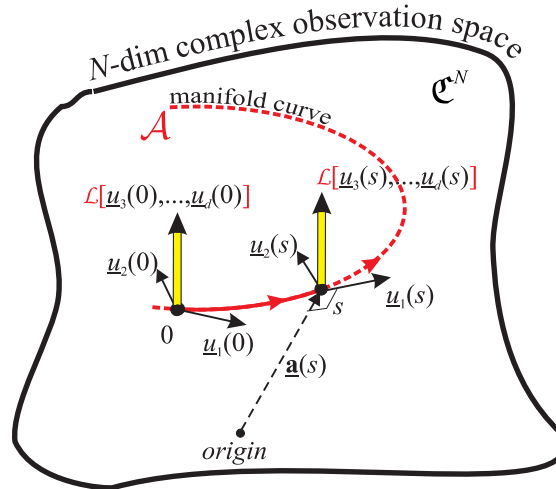
Fig. 3. "Moving frame" $\mathbb{U}(0)$ and $\mathbb{U}(s)$.

E. Curvatures, Cartan matrix and orthogonality

Fundamental Uniqueness Theorem states that for a d-dimensional curve, a total of $d - 1$ *curvatures* are sufficient to uniquely define that curve except its relative position and alignment in space. This leads to the definition of curvatures. Interestingly, expressions for curvatures are linked with the expressions for coordinate vectors in a recursive manner as follows:

$$\kappa_i(s) = \|\underline{u}_i'(s) + \kappa_{i-1}\underline{u}_{i-1}(s)\| \quad (13)$$

$$\underline{u}_i(s) = \frac{\underline{u}'_{i-1}(s) + \kappa_{i-2}\underline{u}_{i-2}(s)}{\kappa_{i-1}} \tag{14}$$

Some of the initial and final values are listed below for convenience:

$$\kappa_1(s) = \|\underline{u}'_1(s)\| \tag{15}$$

$$\kappa_2(s) = \|\underline{u}'_2(s) + \kappa_1\underline{u}_1(s)\| \tag{16}$$

$$\kappa_d(s) = 0 \tag{17}$$

$$\underline{u}_1(s) \triangleq \mathbf{a}'(s) \tag{18}$$

$$\underline{u}_2(s) = \frac{\underline{u}'_1(s)}{\kappa_1} \tag{19}$$

$$\underline{u}_d(s) = \frac{\underline{u}'_{d-1}(s) + \kappa_{d-2}\underline{u}_{d-2}(s)}{\kappa_{d-1}} \tag{20}$$

Plot given in Fig. 4 was obtained for ULA with unity inter-sensor spacing. Note that unity inter-sensor spacing means one half-wavelength distance.

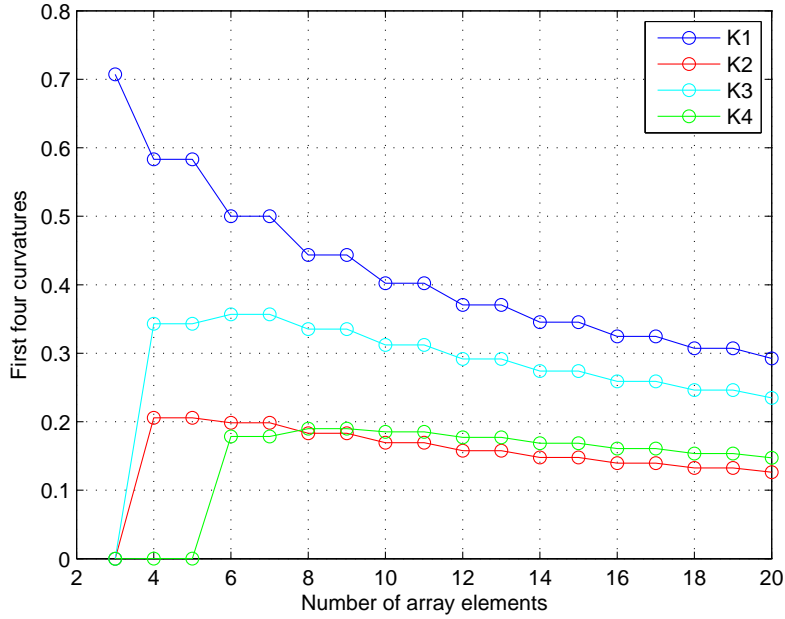Fig. 4. Curvatures of ULA as a function of array elements-N

Further, (14) can be modified and rearranged to get:

$$\underline{u}'_i(s) = \kappa_i(s)\underline{u}_{i+1}(s) - \kappa_{i-1}(s)\underline{u}_{i-1}(s) \tag{21}$$

with

$$\underline{u}'_1(s) = \mathbf{a}''(s) = \kappa_1(s)\underline{u}_2(s) \tag{22}$$

In a more compact form, we can write

$$\mathbb{U}'(s) = \mathbb{U}(s)\mathbb{C}(s) \tag{23}$$

where $\mathbb{C}(s)$ denotes *Cartan Matrix*. This is an important matrix as it contains information about all $d-1$ curvatures which is evident from its expression:

$$\mathbb{C}(s) \triangleq \begin{bmatrix} 0 & -\kappa_1(s) & 0 & \cdots & 0 & 0 \\ \kappa_1(s) & 0 & -\kappa_2(s) & \cdots & 0 & 0 \\ 0 & \kappa_2(s) & 0 & \cdots & 0 & 0 \\ \vdots & \vdots & \vdots & \ddots & \vdots & \vdots \\ 0 & 0 & 0 & \cdots & 0 & -\kappa_{d-1}(s) \\ 0 & 0 & 0 & \cdots & \kappa_{d-1}(s) & 0 \end{bmatrix} \tag{24}$$

Using (12) and (23), it is easy to show that:

$$\mathbb{F}'(s) = \mathbb{F}(s)\mathbb{C}(s) \tag{25}$$

or

$$\mathbb{F}(s) = \mathrm{expm}(s\,\mathbb{C}(s)) \tag{26}$$

Strictly speaking, orthogonality is of two types viz. *wide sense* and *narrow sense* which is defined for any two complex vectors of unit magnitude as follows:

$$\begin{array}{lll} \text{"wide" sense} & \mathrm{Re}(\underline{u}_i^H(s).\underline{u}_j(s)) = 0 & \text{for } i \neq j \\ \text{"narrow" sense} & \underline{u}_i^H(s).\underline{u}_j(s) & \text{for } i \neq j \end{array} \tag{27}$$

For a general linear array, orthogonality in wide sense holds. Only for the special case of symmetrical array, orthogonality in narrow sense holds.

F. Significance of rate of change of arc length

For a linear array, (7) can be simplified to write the steering vector as:

$$\underline{\mathbf{a}}(\phi) = \exp(-j\underline{r}_x \cos(\phi)) \tag{28}$$

The above expression can be easily proved by putting $\theta = 0$. Note that the y and z coordinates of the sensor position vectors are all zero.

Also, (9) can be used to evaluate s which comes out to be in the following form:

$$s(\phi) = \pi\|\underline{r}_x\|(1 - \cos(\phi)) \tag{29}$$

and consequently, following holds true:

$$\dot{s}(\phi) = \pi\|\underline{r}_x\| \sin(\phi) \tag{30}$$

$\dot{s}(\phi)$ is interestingly related to resolution. Given 2 closely placed sources at ϕ_1 and ϕ_2, steering vectors corresponding to both directions can be calculated and if they are situated nearby on the manifold, these two sources are well-resolved otherwise they are not. This is equivalent to saying that high value of $|s(\phi_1) - s(\phi_2)|$ means good resolution and low value means poor resolution. Thus, $\dot{s}(\phi)$ is one measure of comparing resolutions at different DOAs.

Fig. 5 reveals that in a linear array, resolution is better at broadside position (around $\phi = 90°$) rather than at endfire position (around $\phi = 0^o$ or $180°$). Moreover, increasing the number of sensors improves the resolution throughout proportionally, which is quite expected. Note that the array cannot resolve sources at endfire positions due to its cylindrical symmetry.
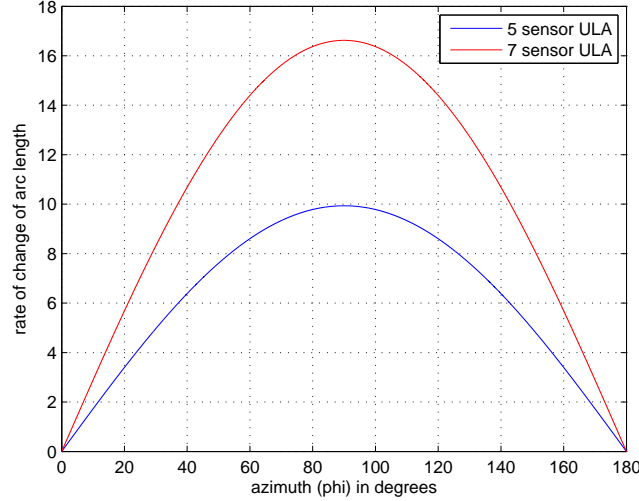
Fig. 5. Variation of $\dot{s}(\phi)$ for ULA of 5 and 7 sensors

G. Manifold Length, $\mathbb{U}_{odd}$ and $\mathbb{U}_{even}$

Another significant parameter is *Manifold Length* which is simply the length of the manifold curve or the value of $s(\phi = 180°)$ which easily comes out to be $2\pi\|\underline{r}_x\|$. Note that in equation (20), if κ_{d-1} becomes equal to zero, then the expression becomes invalid to compute $\underline{u}_d$. This situation arises when a sensor is located at the centroid of the array. In that case, an orthogonalisation procedure is employed to show that the value of $u_d(s)$ actually comes out to be $[0, ..., 1, 0, ..., 0]^T$ with the non-zero entry at the same position as that of the sensor at the centroid in $\underline{r}_x$ vector.

Some other important parameters include $\mathbb{U}_{even}$ and $\mathbb{U}_{odd}$ which are defined as below:

$$\mathbb{U}_{\text{odd}} = [\underline{u}_1(s), \underline{u}_3(s), ..., \underline{u}_{d\text{odd}}(s)] \tag{31}$$

$$\mathbb{U}_{\text{even}} = [\underline{u}_2(s), \underline{u}_4(s), ..., \underline{u}_{d\text{even}}(s)] \tag{32}$$

where

$$d_{\text{odd}} = \lfloor ((d-1)/2) \rfloor + 1 \tag{33}$$

and

$$d_{\text{even}} = \lfloor (d/2) \rfloor \tag{34}$$

H. Inclination angle

Another important concept is that of *inclination angle* ζ_{inc} which is defined as the angle formed between manifold vector $\underline{\mathbf{a}}(s)$ and the subspace $\mathcal{L}[\mathbb{U}_{\text{even}}(s)]$. Mathematically, it can be expressed as:

$$\zeta_{\text{inc}} = \angle(\underline{\mathbf{a}}(s), \mathcal{L}[\mathbb{U}_{\text{even}}(s)]) \tag{35}$$

or equivalently,

$$\cos \zeta_{\text{inc}} = \sqrt{\frac{1}{N} \mathbf{a}^H(s) \mathbb{P}_{U\text{even}} \underline{\mathbf{a}}(s)} = \sqrt{\frac{1}{N} \sum_{i=\text{even}}^{N} \mathbf{a}^H(s) \underline{u}_i(s)} \tag{36}$$

For the special case of symmetrical linear array, inclination angle is $0°$.

Plot given in Fig. 6 was obtained when the rightmost sensor of a symmetrical linear array was disturbed from its position.
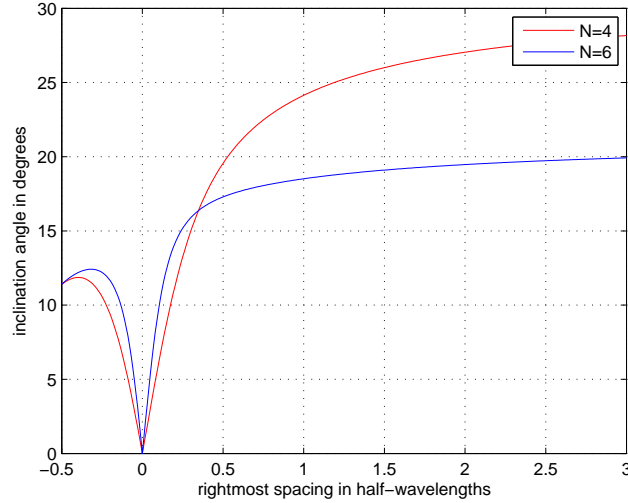
Fig. 6. Inclination angle of linear arrays with N = 4 or 6

I. Manifold Radii Vector

Manifold Radii Vector is defined in the following way:

$$\underline{R} = \begin{cases} [0, -R_2, 0, -R_4, 0, ..., 0, -R_d]^T \\ \text{if } \nexists \text{ sensor at the array centroid} \\ \\ [0, -R_2, 0, -R_4, 0, ..., 0, -R_{d-1}, 1]^T \\ \text{otherwise} \end{cases} \tag{37}$$

with

$$R_2 = \frac{1}{\kappa_1} \text{ and } R_i = \frac{\prod_{n=\text{even}}^{i-2} \kappa_n}{\prod_{n=\text{odd}}^{i-1} \kappa_n} \text{ for } i > 2 \tag{38}$$

An important equation which relates steering vector, coordinate matrix and manifold radii vector is given as follows:

$$\underline{a}(s) = \mathbb{U}(s)\underline{R} = \mathbb{U}(0)\mathbb{F}(s)\underline{R} \text{ where } \mathbb{F}(s) = \text{expm}(s\mathbb{C}) \tag{39}$$

The above expression allows one to write the steering vector in terms of differential geometry parameters. The expression is quite useful in MUSIC and is also exploited later in the report.

J. MUSIC algorithm using differential geometry

MUSIC (MUltiple SIgnal Classification) is a well-known algorithm which processes data captured from sensors ($\underline{x}(t)$) to determine DOAs of signals. Firstly, noise subspace is estimated. Then the manifold is searched over for the steering vectors which are (nearly) orthogonal to the estimated noise subspace. Subspace spanned by such vectors will comprise the signal subspace $\mathcal{L}[\mathbb{A}]$. And once signal subspace is determined, sources can be localised. This whole process is equivalent to taking the intersection of manifold with the subspace orthogonal to the noise subspace. Directions corresponding to the intersection points on the manifold will correspond to the actual DOA of signals. It is clear that the accuracy of DOA estimation is dependent upon how accurately the noise subspace is estimated which, in turn, is dependent upon the SNR and observation interval or the number of snapshots.

Using the model given by (1), theoretical covariance matrix $\mathbb{R}_{xx}$ of array signal vector $\underline{x}(t)$ can be formed

$$\mathbb{R}_{xx} \triangleq \mathcal{E}\{\underline{x}(t)\underline{x}(t)^H\} \in \mathfrak{C}^{N\text{x}N} \tag{40}$$

$$= \mathbb{A}\mathbb{R}_{mm}\mathbb{A}^H + \sigma^2\mathbb{I}_N \tag{41}$$

The above equations can be easily proved by assuming

- $\mathcal{E}\{\underline{x}(t)\} = 0$ or equivalently, zero mean signal
- Noise to be white Gaussian (zero mean)
- $\mathbb{R}_{mm} = \mathcal{E}\{\underline{m}(t)\underline{m}(t)^H\}$.

Practically, only a finite number of snapshots are available, say L. Using that, sample covariance matrix can be formed as follows:

$$\widehat{\mathbb{R}}_{xx} \triangleq \frac{1}{L}\sum_{i=1}^{L}\underline{x}(t_i)\underline{x}(t_i)^H = \frac{1}{L}\mathbb{X}\mathbb{X}^H \tag{42}$$

where

$$\mathbb{X} \triangleq [\underline{x}(t_1), \underline{x}(t_2), ..., \underline{x}(t_L)] \in \mathfrak{C}^{N\mathbf{X}L} \tag{43}$$

Now, if $\mathbb{P}_n$ is taken as projection operator on to the noise subspace (spanned by the noise eigenvectors of the array covariance matrix), the *cost function* can be evaluated as follows:

$$\xi_{\text{MUSIC}}(s) = \underline{\mathbf{a}}^H(s)\mathbb{P}_n\underline{\mathbf{a}}(s) \tag{44}$$

The cost function becomes identically equal to zero whenever any steering vector in the manifold becomes orthogonal to the noise subspace and that particular steering vector will correspond to the actual DOA of the signal. Note that for multiple signals, there will be multiple such vectors.

To further simplify the expression for cost function in (44), we can use the equation (39) and express the manifold in terms of differential geometry parameters in the following manner:

$$\begin{aligned}
\xi_{\text{MUSIC}}(s) &= \underline{\mathbf{a}}^H(s)\mathbb{P}_n\underline{\mathbf{a}}(s) \\
&= \underline{R}^T\mathbb{F}^T(s)\mathbb{U}^H(0)\mathbb{P}_n\mathbb{U}(0)\mathbb{F}(s)\underline{R} \\
&= \text{Tr}\{\mathbb{U}^H(0)\mathbb{P}_n\mathbb{U}(0)\mathbb{F}(s)\underline{R}\,\underline{R}^T\mathbb{F}^T(s)\} \\
&= \text{Tr}\{\overline{\overline{\mathbb{P}}}_n\mathbb{V}(s)\}
\end{aligned} \tag{45}$$

where the matrix $\overline{\overline{\mathbb{P}}}_n \triangleq \mathbb{U}^H(0)\mathbb{P}_n\mathbb{U}(0)$ is a constant hermitian matrix and termed as the *orientation of the noise subspace*. Whereas the matrix $\mathbb{V}(s)$ is a real $d \times d$ symmetric matrix depending only on the curvatures.

III. DIFFERENTIAL GEOMETRY OF ARRAY MANIFOLD SURFACES

This section predominantly deals with two- and three-dimensional arrays. As stated in the previous section that for these kind of arrays, the steering vector $\underline{\mathbf{a}}(\theta, \phi)$ consists of two-parameters namely, ϕ and θ and the manifold geometry will be a surface known as *array manifold surface* which is embedded in an N-dimensional complex space. It is formally defined as follows:

$$\mathcal{M} = \{\underline{\mathbf{a}}(\theta, \phi) \in \mathfrak{C}^N, \forall(\theta, \phi) : \theta, \phi \in \Omega\} \tag{46}$$

where Ω denotes the parameter space. The same way in which the shape of a manifold curve $\mathcal{A}$ is uniquely defined by its curvatures (as explained in previous section), the shape of a manifold surface may be quantitatively expressed in terms of intrinsic geometrical parameters such as the Gaussian curvature $K_G(\theta, \phi)$ at each point on the surface (see Fig. 7(a)) and the geodesic curvature $\kappa_g(\theta, \phi)$ of the curves lying on the surface passing through the point (θ, ϕ) (see Fig. 7(b)).

In order to find out the above mentioned curvatures, the building blocks of surface differential geometry have to be defined such as the *manifold metric* and *Christoffel symbols*.

A. Manifold Metric

Let $\underline{\mathbf{a}} = \underline{\mathbf{a}}(\theta, \phi)$ be the regular parametric representation (i.e. partial derivatives w.r.t θ and ϕ exist, and are unique and continuous) of a surface $\mathcal{M}$ embedded in an *N*-dimensional complex space.
Then the (2×2) real semipositive definite symmetric matrix $\mathbb{G}$, defined as

$$\mathbb{G} \triangleq \begin{bmatrix} ||\underline{\dot{\mathbf{a}}}_\theta||^2 & \text{Re}\left\{\underline{\dot{\mathbf{a}}}_\theta{}^H\underline{\dot{\mathbf{a}}}_\phi\right\} \\ \text{Re}\left\{\underline{\dot{\mathbf{a}}}_\phi{}^H\underline{\dot{\mathbf{a}}}_\theta\right\} & ||\underline{\dot{\mathbf{a}}}_\phi||^2 \end{bmatrix} = \begin{bmatrix} g_{\theta\theta} & g_{\theta\phi} \\ g_{\phi\theta} & g_{\phi\phi} \end{bmatrix} \tag{47}$$

is said to be the *manifold metric* where $\underline{\dot{\mathbf{a}}}_\theta = \dfrac{\partial\underline{\mathbf{a}}}{\partial\theta}$ and $\underline{\dot{\mathbf{a}}}_\phi = \dfrac{\partial\underline{\mathbf{a}}}{\partial\phi}$. Clearly, $\det(\mathbb{G}) > 0$ (by Schwarz's inequality).
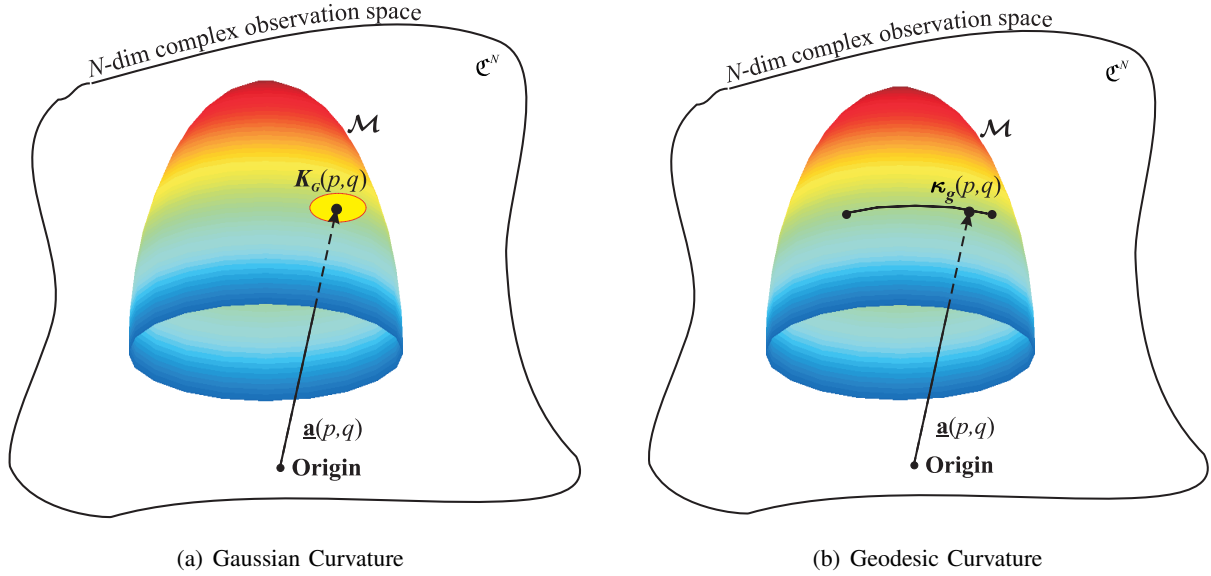
(a) Gaussian Curvature

(b) Geodesic Curvature

Fig. 7. Intrinsic properties of a surface

B. Christoffel Symbol Matrices

The *Christoffel symbols of first kind* represent the inner products between the tangent vectors $\underline{\dot{\mathbf{a}}}_\theta, \underline{\dot{\mathbf{a}}}_\phi$ and their derivatives, and are defined as

$$\Gamma_{i,jk} \triangleq \mathrm{Re}\left\{ \underline{\dot{\mathbf{a}}}_i{}^H \underline{\ddot{\mathbf{a}}}_{jk} \right\} \text{ with } i,j,k = \theta \text{ or } \phi \tag{48}$$

Thus there are eight *Christoffel symbols of first kind* forming the two *Christoffel matrices of the first kind* $\boldsymbol{\Gamma}_{1\theta}$ and $\boldsymbol{\Gamma}_{1\phi}$ defined as follows:

$$\boldsymbol{\Gamma}_{1\zeta} \triangleq \begin{bmatrix} \Gamma_{\theta,\theta\zeta} & \Gamma_{\theta,\phi\zeta} \\ \Gamma_{\phi,\theta\zeta} & \Gamma_{\phi,\phi\zeta} \end{bmatrix} \text{ with } \zeta = \theta \text{ or } \phi \tag{49}$$

Christoffel symbol matrices of second kind are defined as follows:

$$\boldsymbol{\Gamma}_{2\zeta} \triangleq \mathbb{G}^{-1}\boldsymbol{\Gamma}_{1\zeta} = \begin{bmatrix} \Gamma^\theta_{\theta\zeta} & \Gamma^\theta_{\phi\zeta} \\ \Gamma^\phi_{\theta\zeta} & \Gamma^\phi_{\phi\zeta} \end{bmatrix} \text{ with } \zeta = \theta \text{ or } \phi \tag{50}$$

C. Intrinsic Geometry of a Surface

A property of a surface which remains invariant under an isometry (distance preserving map between metric spaces) is called an intrinsic property of the surface. The intrinsic geometry of a surface is completely independent of the space in which the surface lies and is built simply from the properties that are isometric invariant. Following are the two important features of intrinsic geometry.

1) Gaussian Curvature: The Gaussian curvature can be expressed as a function of the metric $\mathbb{G}$ and in terms of the Christoffel matrices elements as follows:

$$K_G(\theta,\phi) = -\frac{1}{\sqrt{\det(\mathbb{G})}} \left(\frac{\partial\left(\frac{\sqrt{\det(\mathbb{G})}}{g_{\theta\theta}}\Gamma^\phi_{\theta\phi} \right)}{\partial\theta} - \frac{\partial\left(\frac{\sqrt{\det(\mathbb{G})}}{g_{\theta\theta}}\Gamma^\phi_{\theta\theta} \right)}{\partial\phi} \right) \tag{51}$$

The sign of the Gaussian Curvature gives a hint of the local shape of the surface in the neighbourhood of point (θ,ϕ). For instance, the surface around a point (θ,ϕ) is locally:

- elliptic, if $K_G(\theta,\phi) > 0$ (the whole neighborhood of the surface at the point considered lies on one side of the tangent hyperplane; e.g, a spherical shape),
- hyperbolic, if $K_G(\theta,\phi) < 0$ (one part of the surface at the point considered lies on one side of the tangent hyperplane and the other part on the other side; e.g, a saddle shape),

- either parabolic or planar (i.e flat), if $K_G(\theta, \phi) = 0$ (there is a straight line of the surface, lying totally on the tangent space; e.g., a cylindrical or planar shape).

If the Gaussian curvature at a point on the manifold is a positive number, the local neighborhood of that point is equivalent to the local neighborhood of a point on a sphere of radius $\sqrt{1/K_G}$.

2) Geodesic Curvature: The general expression for the geodesic curvature κ_g of an arbitrary curve on a surface is rather involved but can be considerably simplified for the special case of constant-parameter curves. Let us denote a "θ-parameter curve" (or simply θ-curve) on the surface $\mathcal{M}$ corresponding to a constant value of $\phi = \phi_o$ as

$$\mathcal{A}_{\theta|\phi_o} = \{\underline{a}(\theta, \phi_o) \in \mathfrak{C}^N, \forall \theta : \theta \in \Omega_\theta, \phi_o = \text{constant}\} \tag{52}$$

and, in a similar way, a "ϕ-parameter curve" (or simply ϕ-curve) as

$$\mathcal{A}_{\phi|\theta_o} = \{\underline{a}(\theta_o, \phi) \in \mathfrak{C}^N, \forall \phi : \phi \in \Omega_\phi, \theta_o = \text{constant}\} \tag{53}$$

Different values of ϕ_o(or θ_o, accordingly) generate a family of curves having the same properties covering the entire manifold surface $\mathcal{M}$. Thus, there are two such families of curves providing two alternative ways of treating the manifold surface. These are

- the family of θ-parameter curves

$$\mathcal{M} = \{\mathcal{A}_{\theta|\phi_o}, \forall \phi_o : \phi_o \in \Omega_\phi\} \tag{54}$$

- the family of ϕ-parameter curves

$$\mathcal{M} = \{\mathcal{A}_{\phi|\theta_o}, \forall \theta_o : \theta_o \in \Omega_\theta\} \tag{55}$$

Both families of θ- and ϕ-curves can be used to interpret the manifold surface $\mathcal{M}$ but different parameterization of the surface provide families of curves with different properties.

Now, the geodesic curvature of θ- and ϕ-curves can be defined as follows:

$$\kappa_{g,\theta} \triangleq \kappa_g(\theta, \phi_o) = \sqrt{\frac{\det(\mathbb{G})}{g_{\theta\theta}^3}} \Gamma_{\theta\theta}^{\phi_o} \qquad \kappa_{g,\phi} \triangleq \kappa_g(\theta_o, \phi) = -\sqrt{\frac{\det(\mathbb{G})}{g_{\phi\phi}^3}} \Gamma_{\phi\phi}^{\theta_o} \tag{56}$$

The Concept of Geodicity: It is known that the curve with the minimum length between two points in an Euclidean space is a straight line. This concept when extended to a curve connecting two points on a surface, the curve of minimum length belonging to that surface is called a geodesic curve. If the geodesic curvature of a curve is zero at every point along its length, then it is a geodesic curve and the converse is also true. In short

$$\text{geodesic curve} \Leftrightarrow \text{a curve with } \kappa_g = 0 \tag{57}$$

IV. NON-LINEAR ARRAYS: MANIFOLD PARAMETERS

The manifold vector of an array of N omnidirectional sensors of arbitrary geometry is

$$\underline{a}(\theta, \phi) = \exp(-j\mathbf{r}^T \underline{k}(\theta, \phi)) \text{ where } (\theta, \phi) \in \Omega \tag{58}$$

where Ω (parameter space) is the field of view (FOV) of the array of sensors.

A. 3D-grid Arrays of Omnidirectional Sensors

A three-dimensional array geometry of omnidirectional sensors is said to be a *3D-grid array* if and only if the following expression is satisfied:

$$\mathbf{rr}^T = \rho^2 \mathbb{I}_3 \text{ where } \rho \in \mathcal{R} \tag{59}$$

This implies that in 3D-grid arrays the vectors $\underline{r}_x, \underline{r}_y$ and $\underline{r}_z$ are orthogonal and also have the same magnitude.

Table I compiles the results of the array manifold parameters for 3D-grid arrays. Based on the results presented in the table, the following comments can be made:

- the Gaussian curvature K_G is always positive and constant. This implies that the manifold surface of a 3D-grid array of N omnidirectional sensors is spherical with radius $\pi\rho$ embedded in an N-dimensional complex space
- the geodesic curvature of the θ-curve ($\kappa_{g,\theta}$) is zero which implies that the θ-curve is a geodesic curve
- the off-diagonal elements of the manifold metric $\mathbb{G}$ (i.e. $g_{\theta\phi}, g_{\phi\theta}$) are zero and hence the θ- and ϕ-curves are orthogonal.

TABLE I
MANIFOLD PARAMETERS OF 3D-GRID ARRAYS.

Intrinsic Parameter	Expression
$\mathbb{G}$	$\rho^2 \pi^2 \begin{bmatrix} 1 & 0 \\ 0 & \sin^2 \theta \end{bmatrix}$
$\det(\mathbb{G})$	$\rho^4 \pi^4 \sin^2 \theta$
$\mathbf{\Gamma}_{1\theta}$	$\rho^2 \pi^2 \cos \theta \sin \theta \begin{bmatrix} 0 & 0 \\ 0 & 1 \end{bmatrix}$
$\mathbf{\Gamma}_{1\phi}$	$\rho^2 \pi^2 \cos \theta \sin \theta \begin{bmatrix} 0 & -1 \\ 1 & 0 \end{bmatrix}$
$\mathbf{\Gamma}_{2\theta}$	$\begin{bmatrix} 0 & 0 \\ 0 & \cot \theta \end{bmatrix}$
$\mathbf{\Gamma}_{2\phi}$	$\begin{bmatrix} 0 & -\cos \theta \sin \theta \\ \cot \theta & 0 \end{bmatrix}$
K_G	$\dfrac{1}{\rho^2 \pi^2}$
$\kappa_{g,\theta}$	0
$\kappa_{g,\phi}$	$\dfrac{\cot \theta_o}{\rho \pi}$

B. Development of manifold surfaces

"Development" is a technique of realising a surface embedded in higher dimension like in $\mathfrak{C}^N$ on to a lower dimension space like $\mathcal{R}^2$. It is a local geodesic mapping in which the higher dimensional surface is mapped to $\mathcal{R}^2$ curve-by-curve. Since the manifold surface can be seen as collection of θ-curves or ϕ-curves, the technique of "development" can be used to "develop" one of the family of curves mentioned above.

In Fig. 8, a curve (expressed in terms of a parameter t) has been mapped to $\mathcal{R}^2$ using "development". Note that the curvature of the developed curve $\kappa_d(t)$ equals the geodesic curvature $\kappa_g(t)$ of the original curve for all t. The motivation behind the conservation of the geodesic curvatures is to maintain the behaviour that the shortest path between two points on the surface maps to a straight line on the plane.
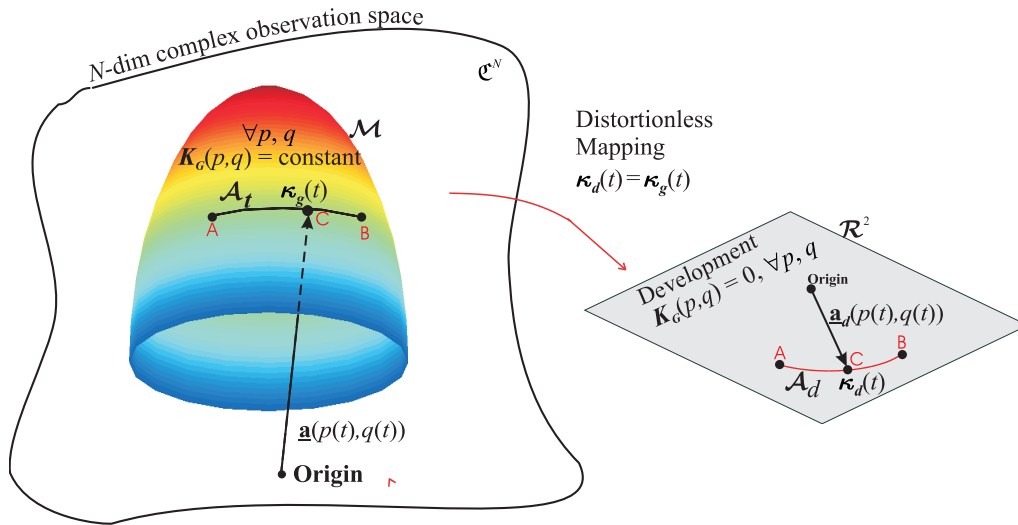

Fig. 8. The concept of "development".

The image of a point (θ, ϕ) lying on the manifold surface, on the real parameter plane for a 3D-grid array simplifies to the following expression:

$$\underline{D}(\theta, \phi) = \rho\pi \tan\theta_o \begin{bmatrix} \sin\phi \\ -\cos\phi \end{bmatrix} \tag{60}$$

The locus of the images $\underline{D}(\theta, \phi)\forall(\theta, \phi)$ is called the *development of the manifold* and has the following properties:

- It exists if and only if the Gaussian curvature of the manifold surface is constant (which is true for a 3D-grid array).
- The curvature of the ϕ-curves on the development is equal to the geodesic curvature $\kappa_{g,\phi}(\theta_o, \phi)$ of the ϕ-curves on the manifold surface.
- For a 3D-grid array (see Fig. 9),
  - the development of ϕ-curves are circular implying constant geodesic curvature of ϕ-curves
  - the development of θ-curves (which are geodesic curves on the surface) are straight lines.
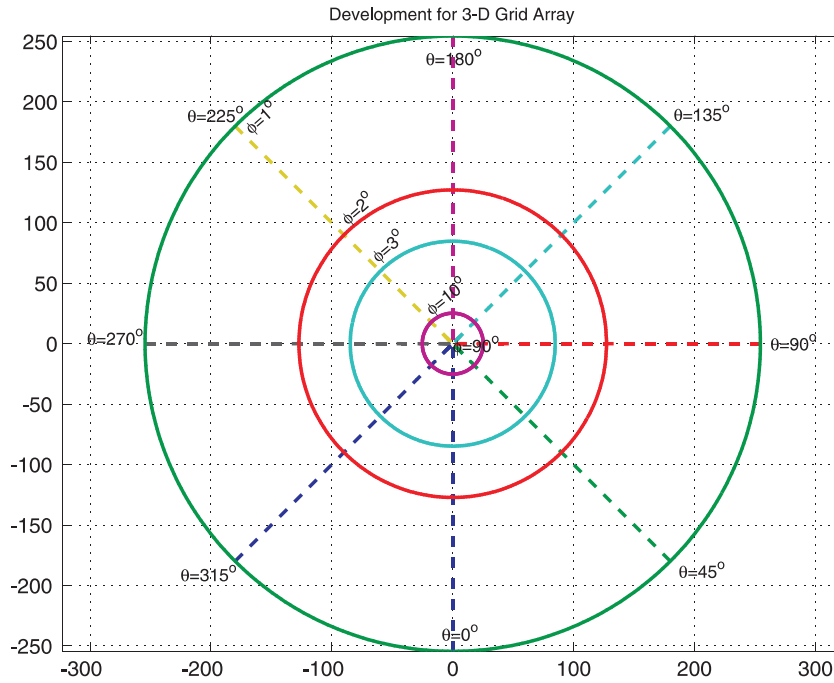

Fig. 9. θ-curves and ϕ-curves development of the manifold of a 3D-grid array with sensors located on the eight vertices of a cube of side one half-wavelength and with reference point the centre of the cube (array centroid).

V. ARRAY BOUNDS

A. Circular approximation of manifold curves

Visualisation of a curve with dimensionality greater than three is impossible. One intuitive way of doing that is *circular approximation* which states that for a sufficiently small neighbourhood of a point $\breve{s}$ on a curve in an N-dimensional space (where the coordinate vectors are strictly orthogonal) can be approximated by a *circular arc*. This circular arc provides an informative notion of the curve's shape in the neighbourhood of point $\breve{s}$ and lie on the plane:

$$\mathcal{H}_{12} \triangleq \mathcal{L}([\underline{u}_1(\breve{s}), \underline{u}_2(\breve{s})]) \tag{61}$$

with the vector $\underline{u}_1(\breve{s})$ as its tangent and radius $R = \kappa_1^{-1}$. The approximation also provides a 2D representation with the curve having main components along the first two coordinate vectors $\underline{u}_1(\breve{s})$ and $\underline{u}_2(\breve{s})$ (see Fig. 10). Note that the coordinate vectors $\underline{u}_1(\breve{s})$ and $\underline{u}_2(\breve{s})$ are not, in general, strictly orthogonal. Therefore, the radius of circular approximation is $\hat{\kappa}_1^{-1}(\breve{s})$ which accounts the "orientation" of the manifold curve $\mathcal{A}$ by the following expression:

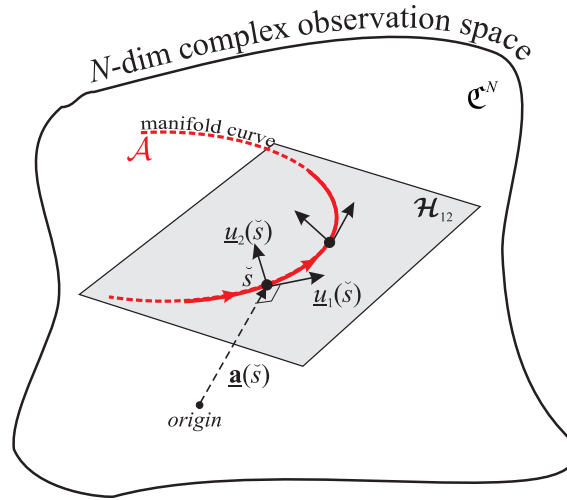$$\hat{\kappa}_1 = \kappa_1 \sin(\zeta) \tag{62}$$

Fig. 10. $\mathcal{H}_{12}$ subspace used to approximate the array manifold at a local level

where ζ is the angle between $\underline{u}_1(\check{s})$ and $\underline{u}_2(\check{s})$. Also,

$$\sin(\zeta) = \sqrt{1 - |\underline{u}_1^H(s)\underline{u}_2(s)|^2} \tag{63}$$

For linear arrays, the value of coordinate vectors can be calculated and substituted to arrive at the following result:

$$\hat{\kappa}_1 = \sqrt{\kappa_1^2 - |\underline{1}_N^T \tilde{r}^3|^2} \quad \text{with} \quad \underline{\tilde{r}} = \underline{r}/\|\underline{r}\| \tag{64}$$

B. Cramer Rao Lower Bound (CRLB)

CRB sets a lower bound on the error covariance matrix of any unbiased estimate, $\hat{p}$, of the true parameter vector $\underline{p} \in \mathcal{R}^M$ in the signal model of (1).

For the case of an array of N sensors receiving M narrowband signals with additive sensor noise of power σ^2, and for a sufficiently large number of snapshots ($L >> 1$), the expression for the deterministic CRB has been shown to be as follows:

$$\text{CRB}[\underline{p}] = \frac{\sigma^2}{2L}(\text{Re}(\mathbb{H} \odot \mathbb{R}_m^T))^{-1} \in \mathcal{R}^{M \times M} \tag{65}$$

where

$$\begin{aligned}
\mathbb{H} &= \dot{\mathbb{A}}^H \mathbb{P}_\mathbb{A}^\perp \dot{\mathbb{A}} \in \mathfrak{C}^{M \times M} \\
\mathbb{R}_m^T &= \mathcal{E}\{m(t)m(t)^H\} \in \mathfrak{C}^{M \times M} \text{ (source covariance matrix)}
\end{aligned} \tag{66}$$

with

$$\begin{aligned}
\mathbb{A} &= [\underline{a}_1, \underline{a}_2, ..., \underline{a}_M] \\
\dot{\mathbb{A}} &= [\underline{\dot{a}}_1, \underline{\dot{a}}_2, ..., \underline{\dot{a}}_M] \\
\mathbb{P}_\mathbb{A}^\perp &= \mathbb{I}_N - \mathbb{A}(\mathbb{A}^H \mathbb{A}^{-1})\mathbb{A}^H
\end{aligned} \tag{67}$$

Following assumptions have been made:

- $N > M$ and the manifold vectors are independent
- Noise is zero mean, temporally white Gaussian process
- $\mathcal{E}\{\underline{n}(t)\underline{n}^H(t)\} = \sigma^2 \mathbb{I}_N$
- Parameters other than $\underline{p}$ are known *a priori*

C. Single emitter CRB

For an array receiving signal from a single source, its power can be expressed as:

$$P = \mathcal{E}\{m(t)m^*(t)\} \tag{68}$$

Using (65), CRB for the bearing p can be expressed as:

$$\mathrm{CRB}[p] = \frac{\sigma^2}{2LP} \frac{1}{\dot{\underline{\mathbf{a}}}^H(p)\mathbb{P}^{\perp}_{\underline{\mathbf{a}}}\dot{\underline{\mathbf{a}}}(p)} \tag{69}$$

Using

$$\dot{\underline{\mathbf{a}}}(p) = \underline{u}_1(s)\dot{s}(p) \quad \text{and} \quad \|\underline{u}_1(s)\| = 1 \tag{70}$$

Also, from (18), it is clear that $\underline{u}_1(s)$ is orthogonal to $\underline{\mathbf{a}}(p)$ and therefore, $\mathbb{P}^{\perp}_{\underline{\mathbf{a}}}\underline{u}_1(s) = \underline{u}_1(s)$. Thus, (69) can be simplified as follows:

$$\mathrm{CRB}[p] = \frac{\sigma^2}{2LP\dot{s}(p)^2} \frac{1}{\underline{u}_1^H(s)\mathbb{P}^{\perp}_{\underline{\mathbf{a}}}\underline{u}_1(s)} = \frac{\sigma^2}{2LP\dot{s}(p)^2} = \frac{1}{2(\mathrm{SNR} \times L)\dot{s}(p)^2} \quad \text{where } \mathrm{SNR} = P/\sigma^2 \tag{71}$$

TABLE II
RATE OF CHANGE OF ARC-LENGTH FOR LINEAR AND PLANAR ARRAYS

Array	Curve $\mathcal{A}$	Rate of change of arc-length s	Parameter p
Linear	$\mathcal{A}$	$\dot{s}(\phi) = \pi\|\underline{r}_x\|\sin\phi$	$p = \phi$
Planar (ϕ, θ)	$\mathcal{A}_{\theta\|\phi_o}$	$\dot{s}(\theta) = \pi\|\underline{r}(\phi_o)\|\cos\theta$	$p = \theta$
	$\mathcal{A}_{\phi\|\theta_o}$	$\dot{s}(\phi) = \pi\|\dot{\underline{r}}(\phi)\|\sin\theta_o$	$p = \phi$

For a linear array, there is only one parameter which is azimuth. Hence, there can be only one CRB value known as *azimuthal CRB* which was plotted for a symmetrical linear array with $r = [\text{-2.5}; \text{-1.5}; \text{-0.5}; 0.5; 1.5; 2.5]$ (See Fig. 11). As can be noted, linear arrays faces difficulty in resolving signals arriving from endfire positions.
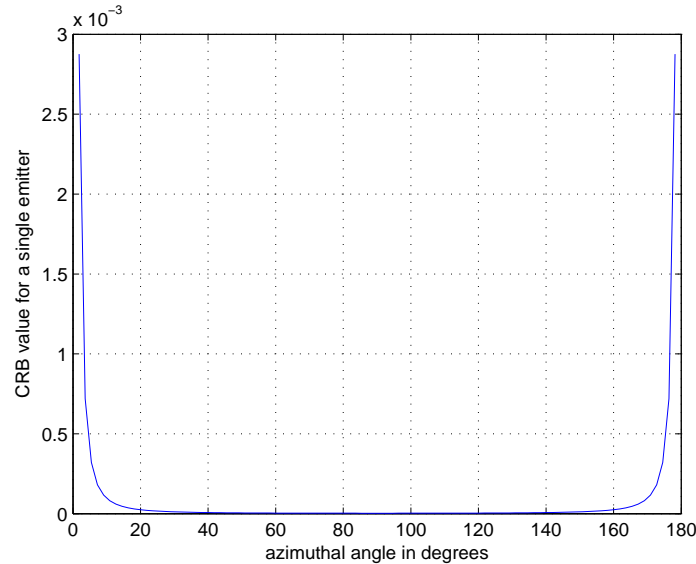

Fig. 11. Azimuthal CRB for a symmetrical linear array

As stated before, in the case of two- and three-dimensional arrays, there are two parameters involved in the steering vector and hence, for each point (θ, ϕ) in the FOV, there will be two values of CRB involved and hence

two surface plots for azimuth and elevation covering the whole FOV will be required which will be called as *azimuthal CRB* and *elevation CRB* plots respectively.

For a UCA with 24 sensors (centroid at origin), its azimuthal and elevation CRB plots for single source are shown in Fig. 12.

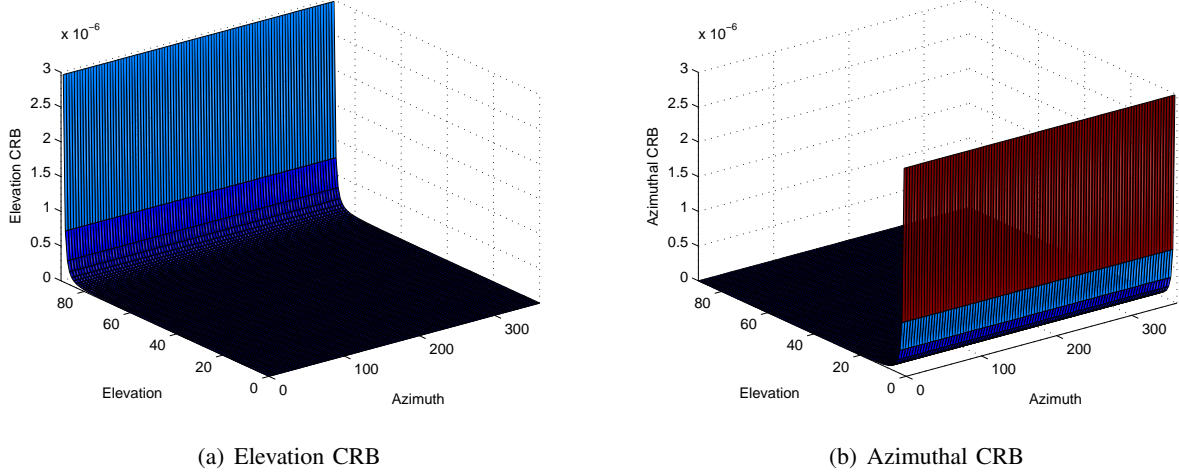(a) Elevation CRB   (b) Azimuthal CRB

Fig. 12. CRB plots for elevation and azimuthal CRB for a 24-sensor UCA

It is clear from Fig. 12 that error in estimating elevation (or equivalently, elevation CRB) is high when elevation is $90°$. Similarly, the error in estimating azimuth is high when elevation around $0°$. And, as expected, the above observations are independent of azimuth.

D. Two emitter CRB

CRB for a two emitter scenario is different from the case of a single emitter. CRB for calculating the DOA of signal from first source will be affected by the presence of the other source. Consequently, the CRB plots for any of the sources will not be independent unless they are sufficiently apart.

For two independent sources, expression for CRB is given by:

$$\text{CRB}[p_1|\mathcal{A}] = \frac{1}{2(\text{SNR}_1 \times L)} \frac{1}{\underline{\dot{\mathbf{a}}}_1^H \mathbb{P}_{\mathbb{A}}^{\perp} \underline{\dot{\mathbf{a}}}_1} \tag{72}$$

(72) can be simplified by using $\underline{\dot{\mathbf{a}}}(p_1) = \underline{u}_1(s_1)\dot{p}_1$ to get,

$$\text{CRB}[p_1|\mathcal{A}] = \frac{1}{2(\text{SNR}_1 \times L)} \frac{1}{\dot{s}(p_1)^2 \underline{u}_1^H(s_1)\mathbb{P}_{\mathbb{A}}^{\perp}\underline{u}_1(s_1)} \tag{73}$$

Fig. 13 shows the azimuthal CRB for the same linear array of previous section. In this particular figure, azimuth for one source has been arbitrarily fixed at $60°$ and the CRB for estimating the azimuth of other source has been plotted while varying it over a range of $0° - 20°$. It can be clearly seen that when the sources are kept near, the value of azimuthal CRB of either of them is quite high irrespective of their azimuth, which is expected.

E. Detection and resolution thresholds

"Detection" capability of an array is given by its ability to identify the number of sources, M while "resolution" means estimating the DOAs of the detected signals. There can be situations when array can tell the number of sources but not their precise locations. To further develop the theory, *detection* and *resolution subspaces* have been defined which will be useful later:

$$\text{detection:} \quad \mathcal{H}_{\text{det}} \triangleq \mathcal{L}([\underline{\mathbf{a}}(\check{s}), \mathbb{P}_{\mathbb{A}}\underline{\mathbf{a}}(\check{s})]) \tag{74}$$

$$\text{resolution:} \quad \mathcal{H}_{\text{res}} \triangleq \mathcal{L}([\underline{\mathbf{a}}(\check{s}), \underline{u}_1(\check{s})]) \tag{75}$$
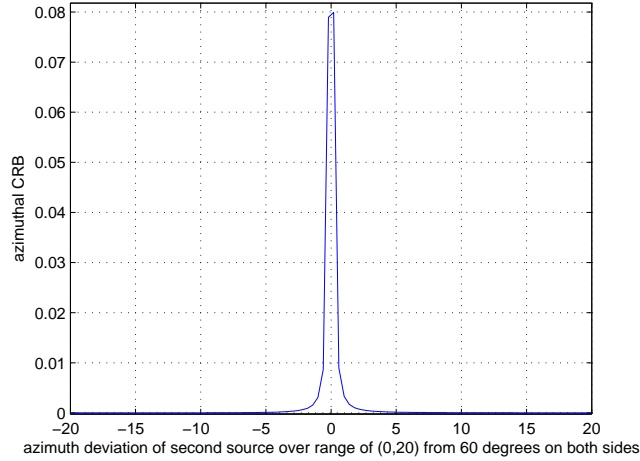
Fig. 13. Azimuthal CRB for one fixed source while moving the other
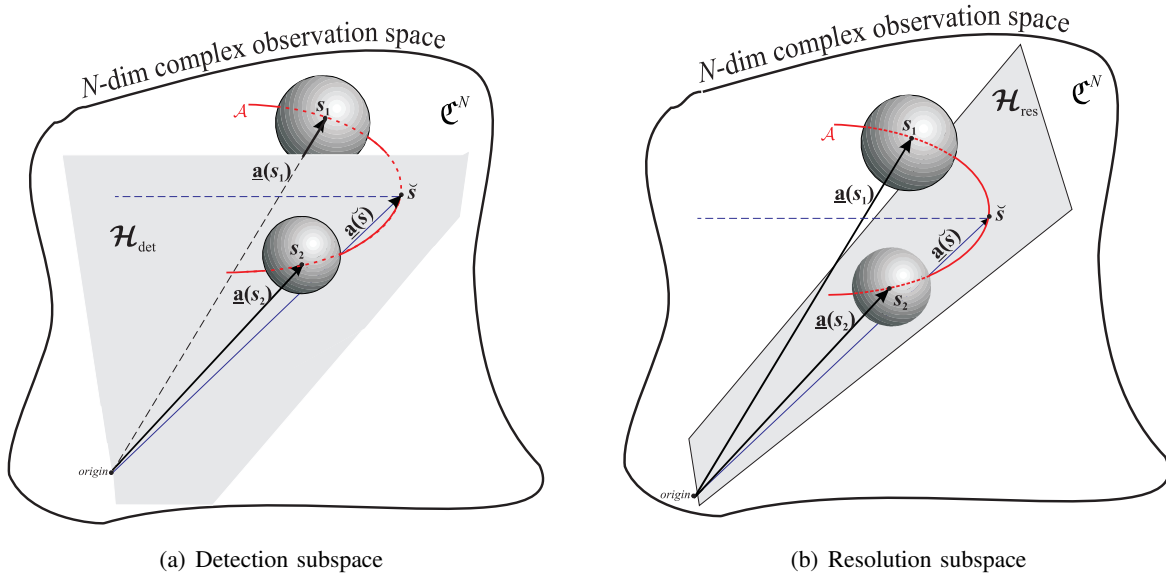

(a) Detection subspace

(b) Resolution subspace

Fig. 14. Depiction of detection and resolution subspace

where $\mathbb{P}_{\mathbb{A}} = \mathbb{A}(\mathbb{A}^H\mathbb{A})^{-1}\mathbb{A}^H$ and $\mathbb{A} = [\underline{\mathbf{a}}(s_1), \underline{\mathbf{a}}(s_2)]$. For convenience, the detection and resolution subspace are shown in Fig. 14.

From a practical view point, any manifold vector $\underline{\mathbf{a}}(s)$ on a manifold curve should not be represented by just a point but a sphere. (known as *uncertainty sphere*) The RMS value σ_{e_i} of the uncertainty due to noise which remains in the system after L snapshots can be represented as an N-dimensional hypersphere of radius σ_{e_i} centred at the manifold vector $\underline{\mathbf{a}}(s_i)$.

F. Estimating detection threshold

Two sources are detected if and only if their uncertainty spheres do not make contact. And the threshold occurs when they just touch each other.

$$\Delta s \geqslant \Delta s_{\text{det-thr}} \tag{76}$$

From Fig. 15, it is clear that

$$\Delta s_{\text{det-thr}} = \hat{\kappa}_1^{-1}\Delta\psi = \frac{\arcsin(\hat{\kappa}_1\sigma_{e_{1,d}}) + \arcsin(\hat{\kappa}_1\sigma_{e_{2,d}})}{\hat{\kappa}_1} \tag{77}$$

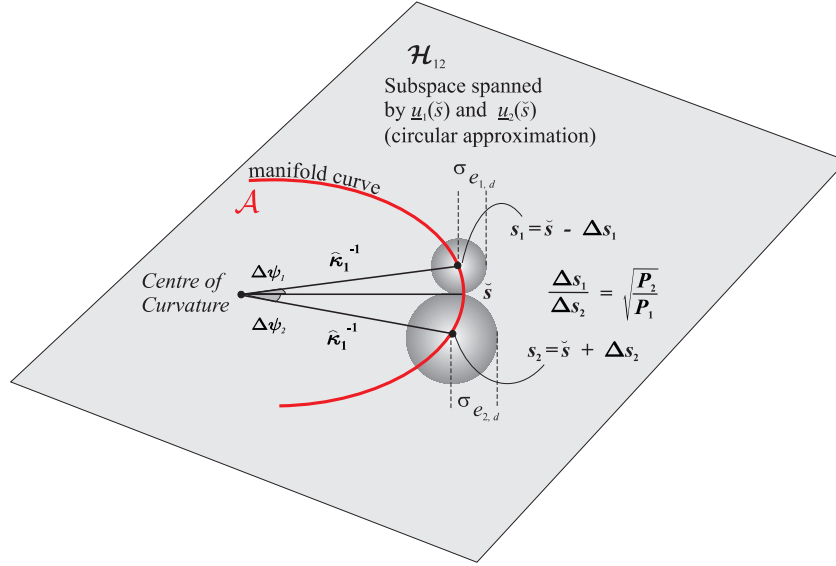Following expressions for the radius of uncertainty spheres can be used:

Fig. 15. Geometry at detection subspace

$$\sigma_{e_{i,d}} = \|\mathbb{P}^\perp_{\mathcal{H}_{\mathrm{det}}}\underline{\mathbf{a}}(s_i)\| = \underline{\mathbf{a}}^H(s_i)\mathbb{P}^\perp_{\mathcal{H}_{\mathrm{det}}}\underline{\mathbf{a}}(s_i) \ \ \mathrm{for} \ \ i=1,2 \tag{78}$$

Thus, the minimum arc-length and angular separation for detection is given the following two expressions (for linear arrays):

$$\Delta s_{\mathrm{det\text{-}thr}} = \sigma_{e_{1,d}} + \sigma_{e_{2,d}} \tag{79}$$

$$\Delta\phi_{\mathrm{det\text{-}thr}} = \frac{1}{\pi\|\underline{r}\|\sin\breve{\phi}}(\sigma_{e_{1,d}} + \sigma_{e_{2,d}}) \tag{80}$$

G. Estimating resolution threshold

Two sources are resolved if their uncertainty spheres do not make contact with the resolution subspace and the threshold occurs when the $\mathcal{H}_{\mathrm{res}}$ is a tangent plane to the uncertainty spheres. Therefore,

$$\Delta s \geqslant \Delta s_{\mathrm{res\text{-}thr}} \tag{81}$$

Once again radius of uncertainty spheres have to be defined:

$$\sigma_{e_{i,r}} = \|\mathbb{P}^\perp_{\mathcal{H}_{\mathrm{res}}}\underline{\mathbf{a}}(s_i)\| \quad \mathrm{for} \quad i=1,2 \tag{82}$$

Using Fig. 16 it can be written that,

$$\Delta s_{\mathrm{res\text{-}thr}} = \Delta s_1 + \Delta s_2 = \hat{\kappa}_1^{-1}\Delta\psi = \frac{\left(\arccos\left(1 - \hat{\kappa}_1\frac{\sigma_{e_{1,r}}}{sin\gamma}\right) + \arccos\left(1 - \hat{\kappa}_1\frac{\sigma_{e_{2,r}}}{sin\gamma}\right)\right)}{\hat{\kappa}_1} \tag{83}$$

Upon simplification, it is easy to show that for a linear array,

$$\Delta s_{\mathrm{res\text{-}thr}} = \sqrt[4]{\frac{4}{\hat{\kappa}_1^2 - \frac{1}{N}}}(\sqrt{\sigma_{e_{1,r}}} + \sqrt{\sigma_{e_{2,r}}}) \tag{84}$$

and,

$$\Delta\phi_{\mathrm{res\text{-}thr}} = \frac{1}{\pi\|\underline{r}\|\sin\breve{\phi}}\sqrt[4]{\frac{4}{\hat{\kappa}_1^2 - \frac{1}{N}}}(\sqrt{\sigma_{e_{1,r}}} + \sqrt{\sigma_{e_{2,r}}}) \tag{85}$$
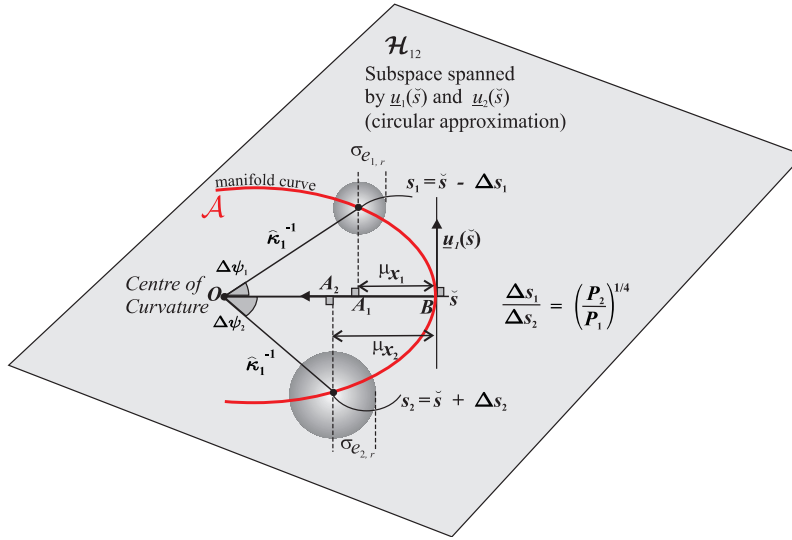
Fig. 16. Geometry at resolution subspace

H. Uncertainty sphere model

Uncertainty sphere represents uncertainty of a steering vector due to noise present in the system. It is possible to reduce noise in the system through two ways:

- High SNR
- High number of snapshots L

That is

$$\sigma_e^2 \propto \frac{1}{L} \quad \text{and} \quad \sigma_e^2 \propto \frac{1}{\text{SNR}} \tag{86}$$

Also, if the efficiency of the DF algorithm is accounted by a term C, it becomes possible to write

$$\sigma_e = \sqrt{\frac{1}{2(\text{SNR} \times L)C}} \tag{87}$$

Using (87) and taking $C = 1$, the expressions for detection and resolution threshold can be simplified as follows:

- Detection threshold:

$$\Delta s_{\text{det-thr}} = \frac{1}{\sqrt{2(\text{SNR}_1 \times L)}} \left(1 + \sqrt{\frac{P_1}{P_2}}\right) \tag{88}$$

- Resolution threshold:

$$\Delta s_{\text{res-thr}} = \sqrt[4]{\frac{2}{(\text{SNR}_1 \times L)\left(\hat{\kappa}_1^2 - \frac{1}{N}\right)}} \left(1 + \sqrt[4]{\frac{P_1}{P_2}}\right) \tag{89}$$

By using $\Delta s = \dot{s}(\breve{\phi})\Delta\phi$ and table II, angular thresholds can be found out for linear and planar arrays.

For instance, for linear arrays, detection and resolution thresholds for azimuth can be written as:

$$\Delta\phi_{\text{det-thr}} = \frac{1}{\pi\|\underline{r}\| \sin\breve{\phi}\sqrt{2(\text{SNR}_1 \times L)}} \left(1 + \sqrt{\frac{P_1}{P_2}}\right) \tag{90}$$

and

$$\Delta\phi_{\text{res-thr}} = \frac{1}{\pi\|\underline{r}\| \sin\breve{\phi}} \sqrt[4]{\frac{2}{(\text{SNR}_1 \times L)\left(\hat{\kappa}_1^2 - \frac{1}{N}\right)}} \left(1 + \sqrt[4]{\frac{P_1}{P_2}}\right) \tag{91}$$

where $\phi_2 = \phi_1 + \Delta\phi$ and $\breve{\phi} = (\phi_1 + \phi_2)/2$.

It is to be noted that,

$$\frac{\Delta\phi_{\text{res-thr}}}{\Delta\phi_{\text{det-thr}}} = \sqrt{\frac{8}{\hat{\kappa}_1^2 - \frac{1}{N}}} \sqrt[4]{\text{SNR} \times L} \gg 1 \tag{92}$$

which reveals that resolution is a more demanding operation. Therefore, if sources are resolved, then usually it means they are detected as well, which is expected.

One interesting thing to note here is that given Δs, it is possible to estimate the number of snapshots required to detect or resolve sources through following expression:

$$L_{\text{det-thr}} = \frac{1}{2\Delta s^2}\left(\frac{1}{\sqrt{\text{SNR}_1}} + \frac{1}{\sqrt{\text{SNR}_2}}\right)^2 \tag{93}$$

and

$$L_{\text{res-thr}} = \frac{2}{\Delta s^4\left(\hat{\kappa}_1^2 - \frac{1}{N}\right)}\left(\frac{1}{\sqrt[4]{\text{SNR}_1}} + \frac{1}{\sqrt[4]{\text{SNR}_2}}\right)^4 \tag{94}$$

VI. SPHERICAL HARMONICS DOMAIN (SHD)

The analysis that has been done till now is done in *spatial domain*, that is the system model considered was in spatial domain and hence the manifold vector and all its differential geometry properties and parameters along with MUSIC was for spatial domain. By using *Spherical Fourier Transform* a new data model can be developed in SHD resulting in a new manifold vector whose differential geometry properties are independent of the array geometry. The next three sections will deal with the system model and MUSIC in SHD followed by the differential geometry of the manifold vector in SHD and a modified MUSIC algorithm based on differential geometry parameters of the manifold.

A. Signal Processing in Spherical Harmonics Domain

The data model used in (1) is a general data model valid for any type of signal. Now, the main focus will be on pressure waves/sound and the existing data model will be modified accordingly.

A narrow-band sound field of L far field sources with wavenumber k, is incident on a spherical array of I microphones of radius r. Let $\underline{\Phi}_i \equiv (\theta_i, \phi_i)$ denote the angular location of the ith microphone $\underline{\Psi}_l = (\theta_l, \phi_l)$ denote the direction of arrival of the lth source. The spatial data model in frequency domain of the sound pressure,

$$\underline{p}(k) = [\underline{p}_1(k), \underline{p}_2(k), ..., \underline{p}_I(k)]^T \tag{95}$$

can be written as

$$\underline{p}(k) = \mathbb{V}(k)\underline{s}(k) + \underline{n}(k) \tag{96}$$

Here, $\mathbb{V}(k)$ is $I \times L$ steering/manifold matrix (same as (2)), $\underline{s}(k)$ is $L \times 1$ vector of signal amplitudes, $\underline{n}(k)$ is $I \times 1$ vector of zero mean, uncorrelated sensor noise. The steering matrix $\mathbb{V}(k)$ is expressed as

$$\mathbb{V}(k) = [\underline{v}_1(k), \underline{v}_2(k), ..., \underline{v}_L(k)] \text{ where } \underline{v}_l(k) = [e^{-j\underline{k}_l^T \underline{r}_1}, e^{-j\underline{k}_l^T \underline{r}_2}, \ldots, e^{-j\underline{k}_l^T \underline{r}_I}]^T \tag{97}$$

The ith term in (97) refers to pressure due to l^{th} unit amplitude plane wave with wave vector $\underline{k}_l$ at location $\underline{r}_i$. This may alternatively be written as
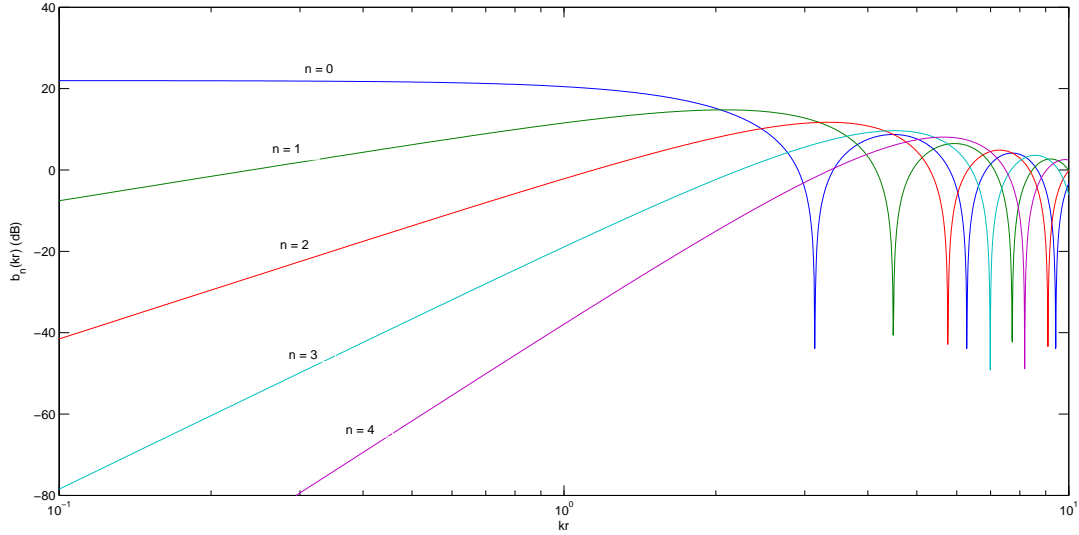
$$e^{-j\underline{k}_l^T \underline{r}_i} = \sum_{n=0}^{\infty} \sum_{m=-n}^{n} b_n(kr) Y_n^{m*}(\underline{\Psi}_l) Y_n^m(\underline{\Phi}_i) \tag{98}$$

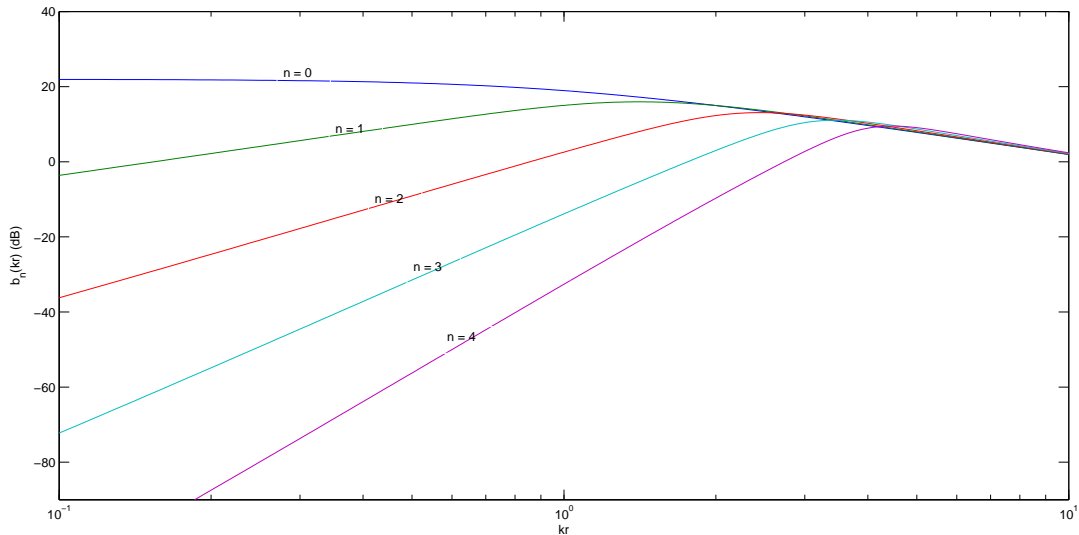where $b_n(kr)$ is called mode strength. The far-field mode strength $b_n(kr)$ is given by

$$b_n(kr) = 4\pi j^n j_n(kr), \text{ for open sphere} \tag{99}$$

$$= 4\pi j^n\left(j_n(kr) - \frac{j_n'(kr)}{h_n'(kr)}\right), \text{ for rigid sphere} \tag{100}$$

where $j_n(kr)$ is spherical Bessel function, $h_n(kr)$ is n^{th} order spherical Hankel function of second kind and $'$ refers to first derivative. (see Fig. 17(a) and 17(b))

(a) open sphere

(b) rigid sphere

Fig. 17. Mode amplitude b_n as a function of kr and n.

In case of a rigid sphere, the mode strength b_n decreases significantly for order greater than kr. Hence, the summation in (98) can be truncated to finite η, called the array order.

The spherical harmonic of order n and degree m, is given by

$$Y_n^m(\theta, \phi) = \sqrt{\frac{(2n+1)(n-m)!}{4\pi(n+m)!}} P_n^m(\cos\theta)e^{jm\phi} \ \forall \ 0 \le n \le \eta, -n \le m \le n \qquad (101)$$

Y_n^m are solution to the Helmholtz equation and P_n^m are associated Legendre functions. The spherical harmonics are used for spherical harmonics decomposition of a square integrable function, similar to complex exponential $e^{j\omega t}$ used for decomposition of real periodic functions.

Substituting (98) in (97), the expression for steering matrix can be written as

$$\mathbb{V}(\underline{\Psi}) = \mathbb{Y}(\underline{\Phi})\mathbb{B}(kr)\mathbb{Y}^H(\underline{\Psi}) \qquad (102)$$

where $\mathbb{Y}(\underline{\Phi})$ is $I \times (\eta + 1)^2$ matrix whose i^{th} row is given as

$$\mathbf{y}(\underline{\Phi}_i) = [Y_0^0(\underline{\Phi}_i), Y_1^{-1}(\underline{\Phi}_i), Y_1^0(\underline{\Phi}_i), Y_1^1(\underline{\Phi}_i), \ldots, Y_\eta^\eta(\underline{\Phi}_i)]. \tag{103}$$

The $L \times (\eta + 1)^2$ matrix $\mathbb{Y}(\underline{\Psi})$ can be expanded on similar lines. The $(\eta + 1)^2 \times (N + 1)^2$ matrix $\mathbb{B}(kr)$ is given by

$$\mathbb{B}(kr) = \mathrm{diag}(b_0(kr), b_1(kr), b_1(kr), b_1(kr), \ldots, b_\eta(kr)). \tag{104}$$

Having introduced the spherical harmonics, the Spherical Fourier Transform (SFT) of the received pressure $p(k, r, \underline{\Phi})$, is given by

$$\begin{aligned} p_{nm}(k, r) &= \int_0^{2\pi} \int_0^\pi p(k, r, \underline{\Phi}) Y_n^{m*}(\underline{\Phi}) \sin(\theta) d\theta d\phi \\ &\cong \sum_{i=1}^I a_i p_i(k, r, \underline{\Phi}_i) Y_n^{m*}(\underline{\Phi}_i) \ \forall \ 0 \le n \le \eta, -n \le m \le n \end{aligned} \tag{105}$$

The spatial sampling of pressure over a spherical microphone array is captured using sampling weights, a_i. The Inverse Spherical Fourier Transform (ISFT) is expressed as

$$\underline{p}(k, r, \underline{\Phi}) \cong \sum_{n=0}^\eta \sum_{m=-n}^n p_{nm}(k, r) Y_n^m(\underline{\Phi}_i) \tag{106}$$

In matrix form, (105) is written as

$$\underline{p}_{nm}(k, r) = \mathbb{Y}^H(\underline{\Phi}) \mathbf{\Gamma} \underline{p}(k, r, \underline{\Phi}) \tag{107}$$

where $\underline{p}_{nm}(k, r) = [p_{00}, p_{1(-1)}, p_{10}, p_{11}, \ldots, p_{\eta\eta}]^T$ and $\mathbf{\Gamma} = \mathrm{diag}(a_1, a_2, \cdots, a_I)$. Also, under the assumption of (105), the following orthogonality property of spherical harmonics holds:

$$\mathbb{Y}^H(\underline{\Phi}) \mathbf{\Gamma} \mathbb{Y}(\underline{\Phi}) = \mathbb{I}_{(\eta+1)^2} \tag{108}$$

where $\mathbb{I}_{(\eta+1)^2}$ is $(\eta + 1)^2 \times (\eta + 1)^2$ identity matrix.

Substituting (102) in (96), then multiplying both side with $\mathbb{Y}^H(\underline{\Phi})\mathbf{\Gamma}$ and utilizing relations (107),(108), we have the following data model in spherical harmonics domain:

$$\underline{p}_{nm}(k, r) = \mathbb{B}(kr) \mathbb{Y}^H(\underline{\Psi}) \underline{s}(k) + \underline{n}_{nm}(k) \tag{109}$$

Multiplying both side of (109) by $\mathbb{B}^{-1}(kr)$, the final spherical harmonics model can be re-written as

$$\underline{a}_{nm}(k, r) = \mathbb{Y}^H(\underline{\Psi}) \underline{s}(k) + \underline{z}_{nm}(k) \tag{110}$$

$$[\underline{a}_{nm}]_{(\eta+1)^2 \times 1} = [\mathbb{Y}^H]_{(\eta+1)^2 \times L} [\underline{s}]_{L \times 1} + [\underline{z}_{nm}]_{(\eta+1)^2 \times 1} \tag{111}$$

$$\text{where} \quad \underline{a}_{nm}(k, r) = \mathbb{B}^{-1}(kr) \underline{p}_{nm}(k, r), \tag{112}$$

$$\underline{z}_{nm}(k) = \mathbb{B}^{-1}(kr) \underline{n}_{nm}(k) = \xi \underline{n}(k), \tag{113}$$

$$\xi = \mathbb{B}^{-1}(kr) \mathbb{Y}^H(\underline{\Phi}) \mathbf{\Gamma} \tag{114}$$

It must be noted that ξ is constant for a given array geometry.

The final data model (110) resembles the very first data model (1) but with some major differences. First, the dimensionality of the vectors has changed from N (number of sensors) to $(\eta + 1)^2$ where η is the array order. Second, the new steering vector $\mathbf{y}^H(\psi)$ is independent of array geometry as it does not contain any term related to the microphone positions (see (103)).

From (103), the SHD steering/manifold vector is written as

$$\underline{\mathbf{y}}^H(\theta, \phi) = [Y_0^0(\theta, \phi), Y_1^{-1}(\theta, \phi), Y_1^0(\theta, \phi), Y_1^1(\theta, \phi), \ldots, Y_\eta^\eta(\theta, \phi)]^H \in \mathfrak{C}^{(\eta+1)^2} \tag{115}$$

B. Differential Geometry of SHD Manifold

The SHD manifold will be a surface embedded in $(\eta + 1)^2$ dimensional complex space and is formally defined as:

$$\mathcal{M}_{SH} = \{\underline{\mathbf{y}}^H(\theta, \phi) \in \mathfrak{C}^{(\eta+1)^2}, \forall(\theta, \phi) : (\theta, \phi) \in \Omega\} \tag{116}$$

where, Ω is the field of view of the microphone array and η is the order limitation.

The SHD manifold can be analyzed for various differential geometry properties using the techniques presented in Section III. The following results have been derived for the SHD manifold surface:

- The surface differential parameters have the form same as that of 3D-grid arrays with

$$\rho\pi \leftrightarrow \frac{1}{4\sqrt{\pi}}(\eta + 1)\sqrt{\eta(\eta + 2)} \tag{117}$$

  that is, if $\rho\pi$ in Table I is replaced by the above expression then the differential geometry parameters for SHD manifold $\mathcal{M}_{SH}$ will be obtained. Conversely, for a given order η a 3D grid array can be found with the above ρ whose microphone positions satisfy (59). (see Appendix A for proof).

- It is known from Unsöld's theorem

$$S_n = \sum_{m=-n}^{n} Y_n^{m*}(\theta, \phi) Y_n^m(\theta, \phi) = \frac{2n + 1}{4\pi} \text{ where } n \in \mathcal{Z} \tag{118}$$

  which implies that

$$||\underline{\mathbf{y}}^H(\theta, \phi)||^2 = \sum_{n=0}^{\eta} S_n = \frac{(\eta + 1)^2}{4\pi} \tag{119}$$

  For a fixed order η, the norm of the manifold vector is constant (independent of θ and ϕ). This means that the manifold lies on a complex $(\eta + 1)^2$ dimensional sphere with radius $\frac{(\eta + 1)}{2\sqrt{\pi}}$.

- The Gaussian curvature of the manifold is also constant for a fixed η (see (117) and Table I). This means that the manifold surface is spherical with radius $\frac{1}{4\sqrt{\pi}}(\eta + 1)\sqrt{\eta(\eta + 2)}$. In other words, the manifold surface is a d dimensional complex sphere lying on a higher dimensional complex sphere.

As in (52) and (53) we can define θ-curve for the SHD manifold as

$$\mathcal{A}_{SH\theta|\phi_o} = \{\underline{\mathbf{y}}^H(\theta, \phi_o) \in \mathfrak{C}^{(\eta+1)^2}, \forall\theta : \theta \in \Omega_\theta, \phi_o = \text{constant}\} \tag{120}$$

and ϕ-curve for the SHD manifold as

$$\mathcal{A}_{SH\phi|\theta_o} = \{\underline{\mathbf{y}}^H(\theta_o, \phi) \in \mathfrak{C}^{(\eta+1)^2}, \forall\phi : \phi \in \Omega_\phi, \theta_o = \text{constant}\} \tag{121}$$

and hence treat the manifold surface either as a family of θ-curves or ϕ-curves.

It can be easily seen that the differentiation of the manifold vector w.r.t ϕ is much more easier than w.r.t θ (calculating higher order derivatives exponential is very cheap while the same for associated Legendre polynomial is a bit involved). Hence the family of ϕ curves will be considered for further analysis.

The ϕ-curve of SHD manifold can be analyzed for various manifold curve parameters like curvatures, moving frame Cartan matrix, etc. using the procedures presented in Section II. The following results have been derived for the ϕ curve (see Appendix B)

- The dimensionality d of the curve is given by

$$d = 3\eta + 1 \tag{122}$$

  which means that the ϕ-curve is situated wholly in some subspace of dimensionality d.

- The arc length of the curve expressed in terms of ϕ is given by

$$s_\phi(\phi) = \left(\frac{1}{4\sqrt{\pi}}(\eta + 1)\sqrt{\eta(\eta + 2)}\sin\theta_o\right)\phi \tag{123}$$

  Clearly, arc length varies linearly with ϕ.

- The moving frame matrix $\mathbb{U}(s)$ is a $(\eta+1)^2 \times d$ matrix whose first 2η columns are given by using the recursive formula of $\underline{u}_i(s)$ and $\kappa_i(s)$ (13),(14). The rest of the column vectors $\underline{u}_{2\eta+1}(s), \underline{u}_{2\eta+2}(s), ..., \underline{u}_{3\eta+1}(s)$ are calculated using an orthogonalization procedure and can be shown to be given by

$$\underline{u}_i(s) = [0, ..., 0, 1, 0, ..., 0]^T \tag{124}$$

where the non-zero entry is at the position where the degree m of the spherical harmonics $Y_n^m(\theta, \phi)$ is zero in the manifold vector $\mathbf{y}^H(\theta, \phi)$.

- The first 2η curvatures are obtained from the calculations of the moving frame matrix. The first $2\eta-1$ curvatures are non-zero and constant (independent of θ and ϕ) and the remaining curvatures $\kappa_{2\eta}, \kappa_{2\eta+1}, ..., \kappa_{3\eta+1}$ are all zero. (If a curvature is zero $\forall (\theta, \phi)$, then all higher order curvatures will be zero)

- The first 2η elements of the radii vector $(d \times 1)$ are calculated using (38) and the remaining ones are $Y_n^m(\theta, \phi)$ evaluated at $m = 0$ and $n = 0, 1, ..., \eta$ i.e

$$\underline{R} = [0, -R_2, 0, -R_4, 0, ..., 0, -R_{2\eta}, Y_0^0(\theta, \phi), Y_1^0(\theta, \phi), ..., Y_\eta^0(\theta, \phi)]^T \tag{125}$$

The rest of the parameters are evaluated directly using (24),(26),(36). After calculating all the parameters of the ϕ-curve, the manifold vector $\mathbf{y}^H(\theta, \phi)$ can be expressed in terms of differential geometry parameters as follows:

$$\mathbf{y}^H(\theta, \phi) = \mathbb{U}(s)\underline{R} = \mathbb{U}(0)\mathbb{F}(s)\underline{R} \quad \text{where } \mathbb{F}(s) = \text{expm}(s\mathbb{C}) \tag{126}$$

C. Detection and Resolution Thresholds

The expressions for detection and resolution thresholds for the arc length on a manifold curve has been already specified in (88) and (89). Also from (123), the rate of change of arc length of the ϕ-curve of the SHD manifold is given by

$$\dot{s}_\phi(\phi) = \frac{1}{4\sqrt{\pi}}(\eta + 1)\sqrt{\eta(\eta + 2)}\sin\theta_o \tag{127}$$

Thus, the expressions for the detection and resolution thresholds for the angular separation can be found out and is given by

$$\Delta\phi_{\text{det-thr}} = \frac{4\sqrt{\pi}}{(\eta + 1)\sqrt{\eta(\eta + 2)}\sin\theta_o\sqrt{2(\text{SNR}_1 \times L)}}\left(1 + \sqrt{\frac{P_1}{P_2}}\right) \tag{128}$$

and

$$\Delta\phi_{\text{res-thr}} = \frac{4\sqrt{\pi}}{(\eta + 1)\sqrt{\eta(\eta + 2)}\sin\theta_o}\sqrt[4]{\frac{2}{(\text{SNR}_1 \times L)\left(\kappa_1^2 - \frac{1}{(\eta+1)^2}\right)}}\left(1 + \sqrt[4]{\frac{P_1}{P_2}}\right) \tag{129}$$

From the above two expressions, it can be seen that the threshold values are minimum at the equator ($\theta_o = 90°$) and maximum at the poles ($\theta_o = 0°, 180°$). This means that the resolving power of a spherical array for two sources placed at the same elevation/latitude is highest at the equator and lowest at the poles which is intuitive because the angle between the wavenumber vectors of the two sources will diminish with the increase in latitude for a given azimuth separation.

Similarly, the threshold values on the θ-curve of the SHD manifold is given by

$$\Delta\theta_{\text{det-thr}} = \frac{4\sqrt{\pi}}{(\eta + 1)\sqrt{\eta(\eta + 2)}\sqrt{2(\text{SNR}_1 \times L)}}\left(1 + \sqrt{\frac{P_1}{P_2}}\right) \tag{130}$$

and

$$\Delta\theta_{\text{res-thr}} = \frac{4\sqrt{\pi}}{(\eta + 1)\sqrt{\eta(\eta + 2)}}\sqrt[4]{\frac{2}{(\text{SNR}_1 \times L)\left(\kappa_1^2 - \frac{1}{(\eta+1)^2}\right)}}\left(1 + \sqrt[4]{\frac{P_1}{P_2}}\right) \tag{131}$$

The above two equations point out that the resolving power is independent of the azimuth in which the two sources are placed which is clear because the angle between the wavenumber vectors of the two sources is just the difference of their latitudes/elevations.

D. Source Localization in Spherical Harmonics Domain

Using the final data model (110), the spherical harmonics MUSIC is given by

$$P_{MUSIC}(\theta, \phi) = \frac{1}{\underline{\mathbf{y}}(\theta, \phi)\mathbb{S}_{a_{nm}}^{NS}[\mathbb{S}_{a_{nm}}^{NS}]^H\underline{\mathbf{y}}^H(\theta, \phi)} \tag{132}$$

where, $\mathbb{S}_{a_{nm}}^{NS}$ is the noise subspace obtained from eigenvalue decomposition of of autocorrelation matrix,

$$\mathbb{S}_{a_{nm}} = \mathcal{E}[\underline{a}_{nm}(k)\underline{a}_{nm}^H(k)]. \tag{133}$$

Now using (126) and (45), (132) can be written as:

$$P_{MUSIC}(\theta, \phi) = (\text{Tr}\{[\mathbb{U}^H(0)\mathbb{P}_n\mathbb{U}(0)] \ [\mathbb{F}(s)\underline{R}\underline{R}^T\mathbb{F}^T(s)]\})^{-1}$$
$$= \frac{1}{\text{Tr}\{\overline{\mathbb{P}}_n\mathbb{V}(s)\}} \tag{134}$$
$$\text{where } \mathbb{P}_n = \mathbb{S}_{a_{nm}}^{NS}[\mathbb{S}_{a_{nm}}^{NS}]^H, \quad \overline{\mathbb{P}}_n = \mathbb{U}^H(0)\mathbb{P}_n\mathbb{U}(0), \quad \mathbb{V}(s) = \mathbb{F}(s)\underline{R}\underline{R}^T\mathbb{F}^T(s).$$

This gives the differential geometry version of MUSIC algorithm in SHD.

Similarly, for the Minimum Variance Distortionless Response (MVDR) method

$$P_{MVDR}(\theta, \phi) = \frac{1}{\underline{\mathbf{y}}(\theta, \phi)\mathbb{S}_{a_{nm}}^{-1}\underline{\mathbf{y}}^H(\theta, \phi)}$$
$$= \frac{1}{\text{Tr}\{\overline{\mathbb{P}}_n\mathbb{V}(s)\}} \tag{135}$$
$$\text{where } \mathbb{P}_n = \mathbb{S}_{a_{nm}}^{-1}, \quad \overline{\mathbb{P}}_n = \mathbb{U}^H(0)\mathbb{P}_n\mathbb{U}(0), \quad \mathbb{V}(s) = \mathbb{F}(s)\underline{R}\underline{R}^T\mathbb{F}^T(s)$$

gives the differential geometry version of MVDR method in SHD.

VII. SIMULATION RESULTS

Various results like "development", CRB-analysis and MUSIC have been presented in this section. An Eigenmike microphone array was used for this purpose. It consists of 32 microphones embedded in a rigid sphere of radius 4.2 cm (see Fig. 18).

Interestingly, the microphone positions of the spherical array form a 3D-grid. Using the angular positions of all microphones as well as the radius of the sphere, $\mathbf{rr}^T$ can be evaluated to give

$$\mathbf{rr}^T = \begin{bmatrix} 188.4692 & 0.0000 & -0.4120 \\ 0.0000 & 188.7380 & 0.1398 \\ -0.4120 & 0.1398 & 187.2728 \end{bmatrix} \text{cm}^2 \cong 13.7^2\mathbb{I}_3 \text{ cm}^2 \tag{136}$$

Going by the definition given in (59), it is clear that the array geometry is a 3D-grid.

"Development" of the manifold for the same is depicted by Fig. 19. The circles represent "developed" ϕ-curves while straight lines represent "developed" θ-curves of the manifold surface of the sensor geometry.

CRB-analysis (single source) for the spherical array is given by Fig. 20. The SNR value and the number of snapshots are taken to be 10 dB and 100 respectively. It can be observed from the graphs that the CRB is nearly constant throughout the FOV (due to spherical symmetry). The reason for some variations over the FOV especially in Fig. 20(a) can be accounted to the use of limited number of microphones. The azimuth CRB (Fig. 20(b)) blows up at the poles ($\theta = 0°$ and $\theta = 180°$) as expected.

The MUSIC spectrum for two sources placed at $(\theta, \phi) = (20°, 50°)$ and $(15°, 120°)$ is simulated for the Eigenmike microphone array using (134) and is shown in Fig. 21.

VIII. CONCLUSION

The concepts of differential geometry have been successfully incorporated in SHD. Also, MUSIC has been implemented for two sources as illustrated in previous section. A new theoretical framework has been suggested to implement MUSIC in a different way by expressing the manifold vector by its differential geometry parameters, which is more realistic and intuitive. The work described in this report has possibly opened new avenues to use differential geometry in DF problems, and probably beyond that. Various issues to ponder regarding the material covered in this report have been listed in the next section.
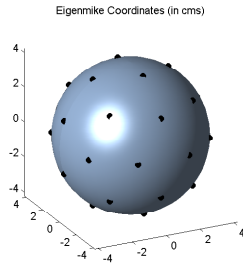
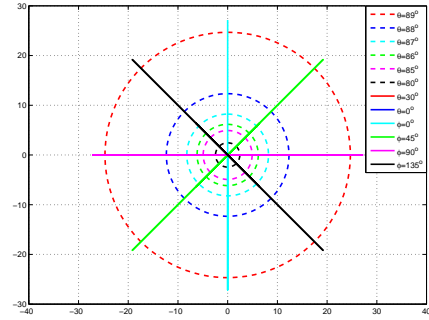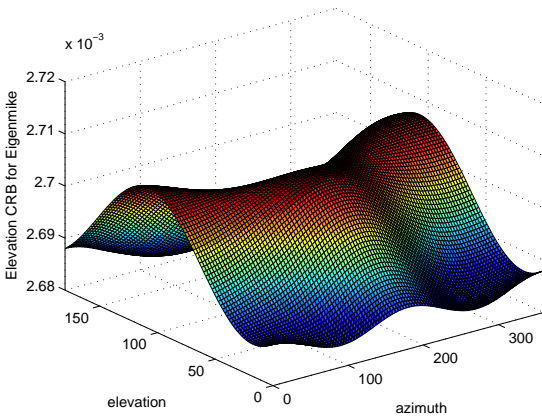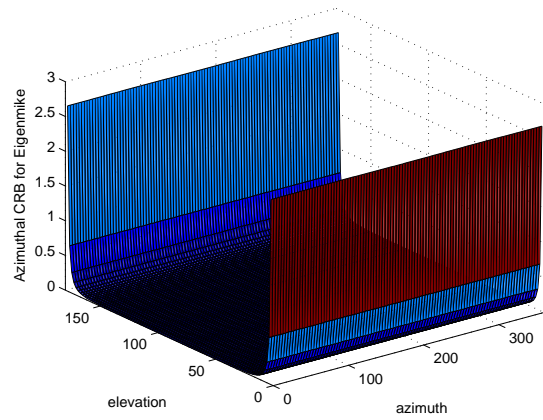Fig. 18. Microphone positions (in cm)

Fig. 19. Development of θ- and ϕ-curves for Eigenmike microphone

(a) Elevation CRB

(b) Azimuth CRB

Fig. 20. CRB-analysis for the spherical array

IX. **FUTURE WORK/ ADVANCEMENTS**

- *Higher dimensional manifold*: The basic motivation behind implementing SH-MUSIC using differential geometry is that the dimensionality of steering vector/ manifold vector in differential geometry version is usually higher than the standard SHD. Normally, $N \geq 32$ and $\eta = 3, 4$ that means the dimensionality of steering vector is $N = 32$ and $(\eta + 1)^2 = 16, 25$ respectively. Consequently, the dimensionality of manifold is higher in the differential geometry version of SHD. This would mean that in DF algorithms like MUSIC where orthogonality of steering vectors corresponding to DOA of incident signals is checked with the noise subspace, the steering vector belonging to higher dimensional manifold can be advantageous in terms of detection/ resolution. Since, the CRB-analysis has not been done for the differential geometry version, there is a scope for improvement of resolution there.

- *Tracking*: Moving sources can be tracked by localising their positions at fixed time intervals. DOA corresponding to each sensor at those fixed intervals can be represented on a real sphere. Those points can be connected by smooth curves to get approximate trajectory of the sources. The real trajectory will correspond to a trajectory of steering vector in complex higher-dimensional space too. Analysis of that complex trajectory can be used to reduce processing required for localising source in the following manner. Depending on the velocity and distance of source from the sensor array, the area on the manifold to be searched to localise source at subsequent time instant can be surprisingly reduced. Clearly, there will not be any discontinuity in source trajectory and hence, by optimisation the possible region, in which the DOA of source at subsequent time instant will lie, can be estimated.

- *RMSE-analysis*: Quite similar to CRB-analysis, RMSE-analysis can be also be done in DSHD which is more
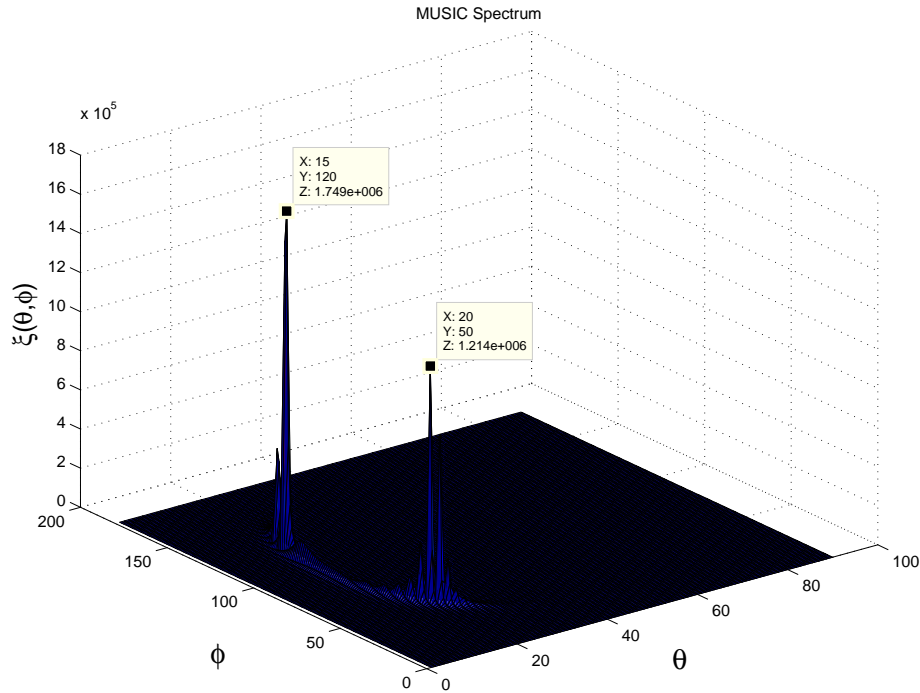
Fig. 21. SH-MUSIC spectrum

realistic than CRB-analysis.

- *Comparison with MVDR*: The analysis done in this report can be compared with performance of other methods such as MVDR, Beamforming etc.
- *Dimensionality reduction*: Various methods exist for realising higher-dimensional data in a lower one (typically 1, 2 or 3). In NLDR, various *manifold learning* algorithms exist like ISOMAP, MDS, PCA, LLE, Hessian LLE, Laplacian, Diffusion Map, LTSA, etc. Similar to these, the concept of "development" has been discussed in this report which is a kind of NLDR method. Every NLDR method has some peculiarity. "Development" uses local geodesic mapping. An in-depth analysis of "development" can suggest improvement in DSH-MUSIC or even allow one to suggest new DF method.
- *Real manifold*: Whether the real and imaginary part of the manifold individually can be meaningful is still unexplored. There is a concept of real representation of manifold for symmetrical arrays. It is defined by the following expression:

$$\underline{\mathbf{a}}_{\text{real}} = \text{expm}(\pi\|\underline{r}\|(1 - \cos\phi)\mathbb{C})\underline{R} \quad \in \mathcal{R}^N \tag{137}$$

and can be plotted for a $r = [-1; 0; 1]$ as shown in Fig.22. These real representations can be further studied to draw meaningful inferences.

APPENDIX A
PROOF OF EQ.117

Appendix one text goes here.

APPENDIX B
ϕ-CURVE DIFFERENTIAL GEOMETRY PARAMETERS

Appendix two text goes here.
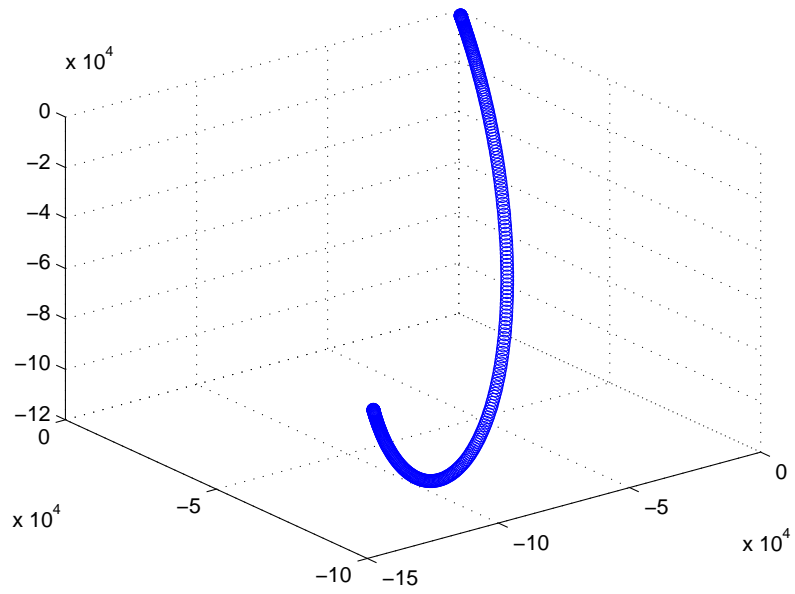
ACKNOWLEDGMENT

The authors would like to thank...

Fig. 22. Real manifold for a symmetrical array with $N = 3$